American Mineralogist, Volume 91, pages 685–701, 2006

Genesis and compositional heterogeneity of smectites. Part III: Alteration of basic pyroclastic rocks—A case study from the Troodos Ophiolite Complex, Cyprus

GEORGE E. CHRISTIDIS*

Technical University of Crete, Department of Mineral Resources Engineering, 73100, Chania, Greece

ABSTRACT

Upper Cretaceous basic pyroclastic rocks, which overlie the Upper Pillow Lavas of the Troodos ophiolitic complex, Cyprus have been altered to bentonites. The resulting smectite is Fe-rich montmorillonite and Fe-rich beidellite, with moderate Mg contents. The smectite is *trans*-vacant and contains abundant exchangeable K. The presence of K is linked with hydrothermal alteration, which affected the higher members of the Troodos ophiolitic suite. The smectite displays significant compositional heterogeneity, which involves substitution of Fe for Al and to a lesser degree substitution of Mg for Al, and that reflects the influence of microenvironmental conditions on smectite formation. The layer charge of the smectite is controlled mainly by the tetrahedral charge, whereas the influence of octahedral charge is of lesser importance, because of Fe for Al substitutions, which does not create a charge deficit. Although the parent pyroclastic rocks were basic, the bentonites contain abundant Si-polymorphs and Si-rich zeolites, from dissolution of abundant radiolarian frustules, which increased the Si-activity of the pore waters, and also produced the partial replacement of smectite by palygorskite at a later stage. Dissolution of frustules was facilitated by the high heat flow from the ocean floor and by the circulation of hydrothermal fluids. The crystal chemistry of smectite and the bulk mineralogy of the bentonites influence the physical properties and industrial applications of the Cyprus bentonites, as well as their response to acid treatment.

Keywords: Troodos ophiolite, Fe-rich montmorillonite, Fe-rich beidellite, layer charge, charge heterogeneity, hydrothermal alteration, bentonite, clinoptilolite

INTRODUCTION

The compositional and structural heterogeneity of dioctahedral smectite in bentonites has been studied thoroughly in the past with various experimental techniques, including X-ray diffraction (XRD), spectroscopy (FTIR, NMR, Mössbauer, and EPR), microcalorimetry, thermal analysis, and electron microprobe analysis (Tettenhorst and Johns 1966; Lagaly and Weiss 1975; Lagaly et al. 1976; Goulding and Talibudeen 1980; Paquet et al. 1982; Talibudeen and Goulding 1983; Nadeau et al. 1985; Lim and Jackson 1986; Decarreau et al. 1987; Iwazaki and Watanabe 1988; Banfield and Eggleton 1990; Christidis and Dunham 1993, 1997; Drits et al. 1998; Cuadros et al. 1999). Although the existence of compositional heterogeneity in Al-rich smectite is well known, the factors that control it are not well understood. Weaver and Pollard (1973) assumed a complete solid solution between beidellite and montmorillonite, but Brigatti and Poppi (1981), Köster (1982), and Yamada et al. (1992) rejected this possibility. Brigatti and Poppi (1981) considered solid solutions among montmorillonite species. Previously, Grim and Kulbicki (1961) had proposed that Wyoming-type and Cheto-type montmorillonite do not form solid solutions. Decarreau et al. (1987) suggested the existence of layers or domains of different composition in Ni-Fe-Mg smectite from lateritic profiles. Finally, Meunier and Velde (1989) proposed a solid solution between high- and low-charged montmorillonite but not between montmorillonite and beidellite.

Christidis and Dunham (1993, 1997) and Christidis (2001) have shown that the chemical characteristics of smectite in bentonites are controlled by the composition of the parent rock and the pore fluid. Smectite derived from intermediate (dacitic-andesitic) precursors is extremely heterogeneous. A compositional transition exists between beidellite and Tatatilla-type (Cheto) montmorillonite, suggesting the possibility of a solid solution between the two species (Christidis and Dunham 1993). In contrast, no transition was observed either between beidellite and Wyoming-type montmorillonite, or between Cheto-type- and Wyoming-type montmorillonite. In contrast, smectite derived from acidic rocks does not necessarily display significant compositional heterogeneity. Compositionally heterogeneous systems are characterized by beidellite and Tatatilla-type montmorillonite (Christidis and Dunham 1997), whereas homogeneous systems may consist of Chambers-type montmorillonite (Christidis 2001). The observed difference in the chemistry of smectite has been attributed to the role of the pore water chemistry (Christidis 2001).

Weathering and/or hydrothermal alteration of basic rocks usually yields dioctahedral Fe-rich smectites including nontronite (Brigatti 1983; Decarreau et al. 1987; Köster et al. 1999) or saponite, which can be Fe-rich or Al-rich (Alt and Honnorez 1984;

* E-mail: christid@mred.tuc.gr

Gillis and Robinson 1990), and, rarely, Mg-rich montmorillonite (Alt et al. 1998). Typical bentonites derived from hydrothermal alteration of basalts containing Fe-rich montorillonite have been described in the Czech Republic (Cicel et al. 1992). In contrast, English bentonites containing also Fe-rich smectite were derived from trachytic rocks (Jeans at al. 1977). Typical Al-rich smectite present in bentonites derived from acidic-intermediate precursors is usually absent from such rocks. Iron-rich smectites, known as non-ideal or abnormal smectite owing to their low dehydroxylation temperatures (Schultz 1969), have *trans*-vacant structures (Drits et al. 1998; Cuadros et al. 1999).

Based on statistical analysis of a large database and the correlation coefficients among the various structural cations of dioctahedral smectites, Güven (1988) proposed that the Mg for Al substitution controls the octahedral compositional characteristics of dioctahedral smectites, whereas the Fe^{3+} for ^{VI}Al substitution does not seem to be significant. In contrast, Christidis and Dunham (1993, 1997), based on microprobe analyses of smectite derived from various types of precursor rocks, found that the Fe^{3+} for ^{VI}Al substitution controls the crystal chemistry of smectite derived from intermediate rocks, whereas the Mg for ^{VI}Al substitution seems to be more important for smectite derived from acidic precursors. The purpose of this contribution is to: (1) examine the compositional heterogeneity and layer charge of smectite in bentonites derived from basic precursors in the Troodos ophiolitic complex, Cyprus; (2) study the mode of formation of the smectite; (3) examine the genetic relationship of smectite with other authigenic phases such as zeolites and Fe- or/and Mn-oxyhydroxides present in the bentonites; and (4) relate the crystal-chemical characteristics of smectite with the physical properties of bentonites.

Geological framework

Geological overview of the Troodos Complex

The Troodos ophiolite complex (Fig. 1), which was emplaced as 90 Ma (Mukasa and Ludden 1987), has a distinctive calc-alkaline character suggesting the presence of a supra-subduction environment (Pearce 1980; Robinson et al. 1983; Moores et al. 1984). The complex consists of the Troodos plutonic unit, the sheeted intrusive unit, and the Troodos pillow lava series from bottom to the top (Fig. 1b). The complex is overlain by pelagic sediments. The plutonic unit forms the core of the complex and consists of ultrabasic rocks and gabbros arranged in a concentric pattern. Owing to substantial post-emplacement uplift, the outer units of the complex represent successively higher levels of the unit (Gass 1980). The sheeted intrusive unit comprises a large number of nearly vertical north-south striking tholeiite dikes. Some of the dikes have a dacitic signature (Thy 1987). Most of the dikes have been hydrothermally altered. The pillow lava series consist of 2–3 km thick basaltic pillow lavas accompanied by minor dikes and flow breccias and have been affected by hydrothermal metamorphism induced by seawater (Spooner et al. 1977; Gillis and Robinson 1990; see also Alt 1999 for a review). The magmatic complex of Troodos is overlain by pelagic sediments of the Paradedi and the Kannaviou formations, which include umbers, radiolarian shales, manganese shales, and mudstones of Campanian-Maastrichtian age, followed by

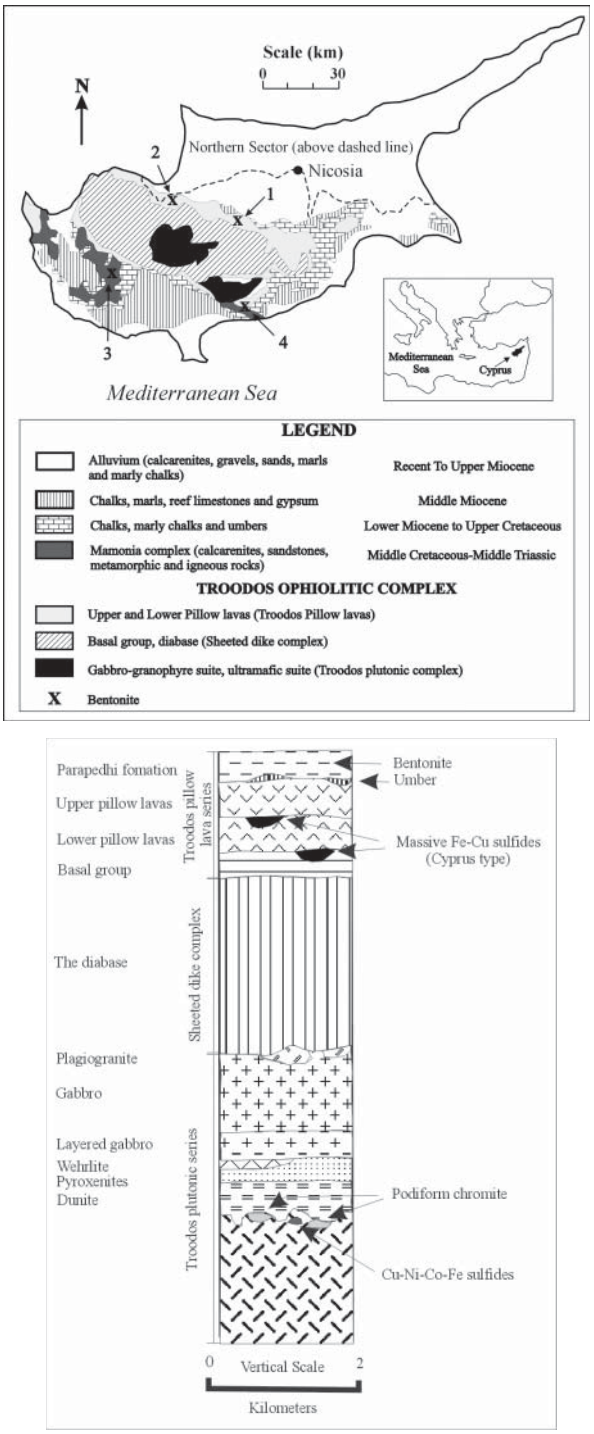

Figure 1. (**a**) Simplified geological map of Cyprus and the location of the bentonite deposits. 1 = Polycanthos deposit, 2 = Skouriotissa deposit, 3 = Kannaviou deposit, and 4 = Moni deposit. (**b**) Schematic stratigraphic column of the Troodos ophiolitic complex.

bentonite beds of similar age. The latter are overlain by a Cretaceous-Triassic melange, which comprises blocks of sandstones, siltstones, and serpentinites embedded in bentonitic clay known as the Moni beds. These sediments are overlain by Paleocene

chalks, then by Miocene reef limestones, and finally by Upper Miocene sediments.

Geology of the bentonites

The deposits occur at the contact between the Upper Pillow Lavas and the overlying carbonate sedimentary rocks and belong to the Perapedi and Kannaviou formations. The bentonites form stratiform, well-compacted bodies with a thickness from a few meters to 40 m depending on the paleomorphology. The bentonites have a waxy appearance when moist and abundant grit content. In places, they contain thin layers (up to 1 cm thick) of opal-CT rich material. Their contact with the underlying pillow lavas and the overlying reef limestones is abrupt. These bentonites have been affected by three fault systems having NS, NE-SW, and EW directions. In the area of Polycanthos (Fig. 1a), four different types of bentonite beds are recognized from top to bottom of the deposit: green-gray bentonite, reddish-ginger bentonite, brown-reddish brown bentonite, and gray bentonite (Fig. 2). In places there are black bentonite horizons, which have been denoted as umbers, i.e., Mn-rich horizons. In some areas, thin layers of a light-green bentonite, denoted as FEO-G in this study, are intercalated with brown-reddish brown bentonite beds.

Materials and methods

Twenty-five samples were obtained from four bentonite deposits (Fig. 1). Samples were collected at a depth of 35–40 cm from the surface to minimize the effect of weathering and contamination caused by mixing of material during excavation operations on active faces. Most samples were collected from the deposit of Polycanthos (Fig. 2). Care was taken to sample the different bentonite horizons. The bulk mineralogy was determined by powder X-ray diffraction (XRD) (Siemens D500, Cu$K\alpha$ radiation, graphite monochromator, 35 kV, and 35 mA, using a 0.02° step size and 1 s per step counting time), on randomly oriented samples initially crushed with a fly press and subsequently ground with pestle and mortar. The clay mineralogy was determined in materials dispersed in distilled water using an ultrasonic probe (20 s). The <2 μm fractions were separated by settling, dried on glass slides at room temperature, and then were solvated with ethylene-glycol vapor at 60 °C overnight to ensure maximum saturation. XRD traces of the clay fractions were obtained using a 0.02° step size and 4 s per step counting time.

Representative clay fractions selected according to their layer charge and charge distribution, determined by electron microprobe analyses (see below), were subdivided into two portions. One portion was saturated twice with K using 1N KCl and the other with 1N $CaCl_2$. The homoionic either K- or Ca-exchanged smectites were centrifuged, dialyzed until chloride free (silver nitrate test), dried on glass slides at room temperature, and then were solvated with ethylene-glycol vapor at 60 °C overnight. Part of the K-saturated fractions was back-saturated with Ca using 1N $CaCl_2$, dried on glass slides at room temperature, and subsequently solvated with ethylene-glycol vapor overnight (Ca-K fractions). The clay fractions were examined with XRD using the conditions described above. In this manner the fraction of the non-swelling, i.e., high-charge smectite, layers is estimated, because usually high-charge layers collapse after K-saturation and do not re-expand after Ca-saturation.

Smectite chemistry was determined by electron microprobe analysis (EPMA) of carbon-coated epoxy impregnated polished blocks, using a JEOL JSM-5600 Scanning Electron Microscope (SEM) equipped with an Oxford Link energy-dispersive spectrometer (EDS). Analyses were performed using 100 s livetime, 10 kV accelerating potential, and 2 nA sample current. A focused beam (ca. 1 μm wide) was used, which yielded an activated area with 2.7 μm diameter. Such an area is sufficiently small to provide information on compositional heterogeneity of smectites. The areas for analysis were selected carefully using back-scattered electron (BSE) images to avoid contamination by Ti and Fe oxides and sulfides and to distinguish coarse-grained minerals (quartz, feldspars) from smectite. Analyses with totals of <70% were discarded following the reasoning of Christidis and Dunham (1993). The totals obtained varied between 73 and 93% and have been attributed to the H_2O content of smectites and to the microporosity between the clay particles (Fig. 3). Volatilization of alkalis, especially Na, invoked by Velde (1984), was not important at the experimental conditions used.

The accuracy, precision, and detection limits of the method used were examined by Dunham and Wilkinson (1978). Briefly, the absolute error for 68% of analyses is ±0.32% for all oxides, whereas the relative error for 68% of the analyses is ±2.3% for oxide concentrations >1% and ±1.9% for oxide concentrations >5%. In general, the accuracy and precision is similar to the WD spectrometers but the detection limits are higher. Although, according to Dunham and Wilkinson (1978), the accuracy and precision decreases for oxide concentrations between 1 and 0.15 wt% (the detection limit for most elements), our work has shown that satisfactory results can be obtained for oxide concentrations as low as 0.45 wt%. Such concentrations are satisfactory for clay mineral analyses.

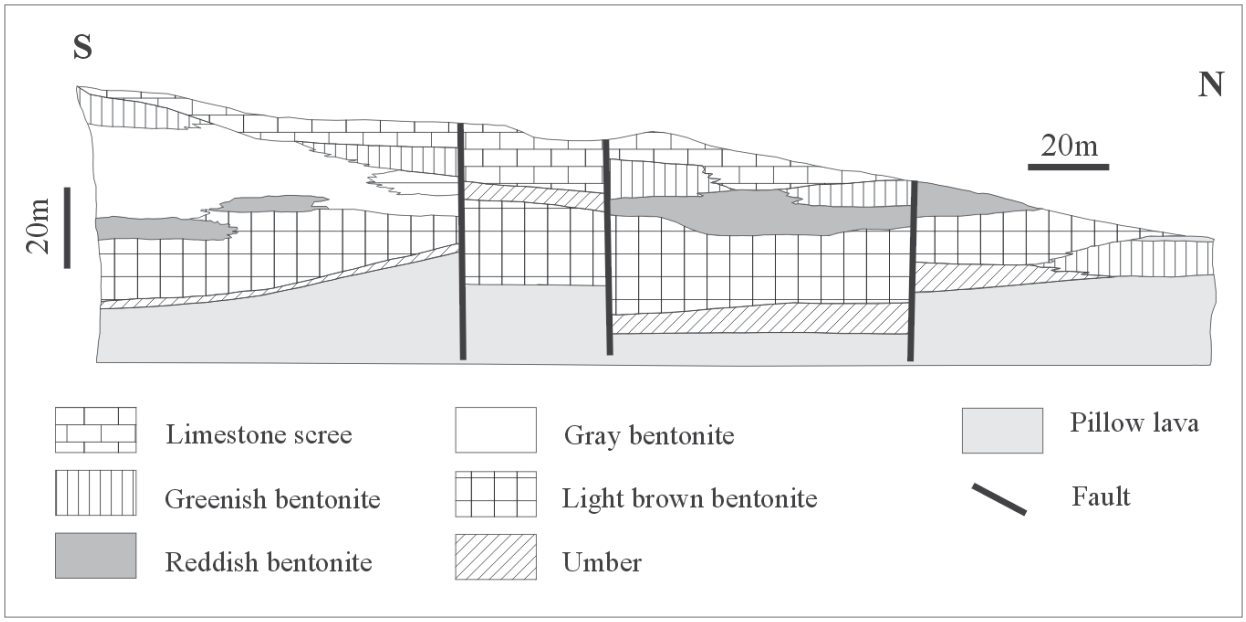

Figure 2. Cross-section of the deposit of Polycanthos with the different bentonite horizons.

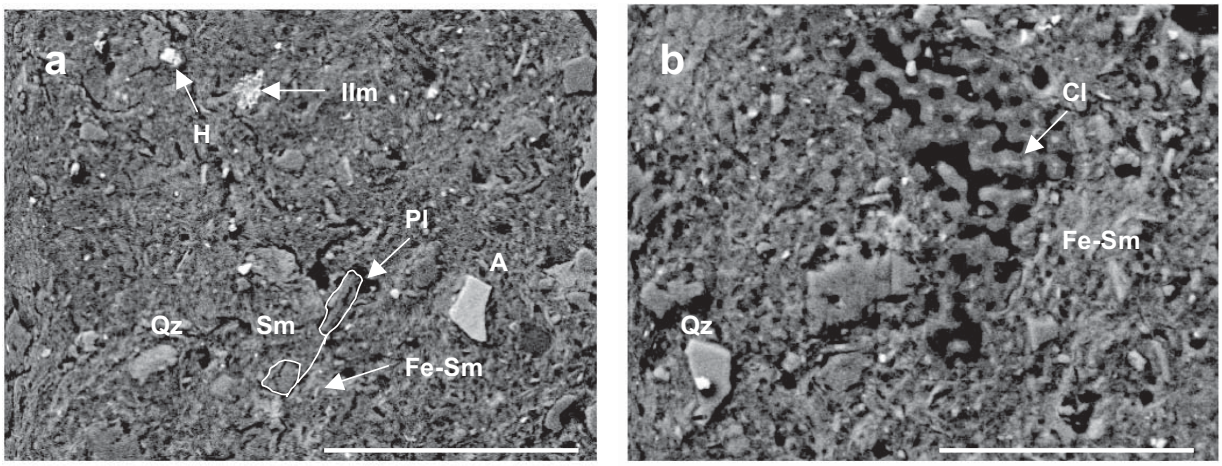

FIGURE 3. Back-scattered electron images of Cyprus bentonites. Note the rough surface caused by the smectite flakes and the difference in relief between soft smectite and harder igneous minerals. (**a**) Smectite (Sm) replaces plagioclase (Pl), Fe-Sm = Fe-rich smectite, Ilm = ilmenite, H = hematite, A = apatite, Qz = quartz, and Pl = plagioclase. Scale bar 60 μm (**b**) Radiolarian frustule is replaced by opal-CT and clinoptilolite (brighter domains labeled Cl). Scale bar 40 μm.

All selected points were analyzed for Si, Ti, Al, Fe, Mn, Mg, Ca, Na, and K. Measured concentrations were automatically corrected for atomic number, absorption in the sample, fluorescence, and dead time (the ZAF correction), using the INCA software of Link. Titanium, when detected, was always associated with ilmenite and consequently was subtracted from the totals. Manganese was always below the detection limit of the instrument. Sample M1 is an exceptional material, containing 3.26 wt% MnO; however, this element is associated with Mn oxides (see results section) and therefore was subtracted from the totals.

The structural formulae of smectites were obtained using 11 O atoms with the following assignments: an amount of Al was assigned in the vacant tetrahedral positions so as to make Si + Al = 4. The remaining Al was assigned to octahedral sites. Iron was assumed to be Fe^{3+}. Inasmuch as a significant number of analyses yielded total number of octahedral cations between 1.987 and 2.00, Mg cations in excess of the ideal dioctahedral occupancy (i.e., 2 cations per half structural formula) were assigned to exchangeable sites. Also Ca, Na, and K were assigned to exchangeable sites. Analyses with more than four Si atoms per half formula unit were considered to be contaminated with free Si polymorphs and were discarded. In general, a minimum of 20 points were analyzed from each sample, except for samples BEN A and APL from the Kanaviou and the Polycanthos deposit, respectively, in which most analyses were contaminated with Si and yielded more than four tetrahedral cations, owing to intimate smectite-opal-CT intergrowths. Similarly, in sample FEO-G, only nine points were analyzed due to the homogeneity of smectite present.

Gold-coated broken surfaces of representative samples were examined with a JEOL JSM-5400 SEM, equipped with an Oxford Link Energy Dispersive Spectrometer (EDS) for qualitative analyses, to determine the textural relationships between the various mineral phases of the bentonites. Infrared (IR) spectra of representative clay fractions were obtained using a Perkin Elmer 1000 Fourier Transform Infrared (FTIR) spectrometer in the range 400–4000 cm^{-1}. Each spectrum was the average of 50 scans collected at 4 cm^{-1} resolution. Precisely 1.5 mg of the smectite clay fractions was diluted in 200 mg KBr and pressed in 13 mm KBr disks, which were subsequently dried at 150 °C. Differential Thermal and Thermogravimetric Analysis (DTA-TG) were performed on clay fractions using a Setaram DTA-TG analyzer. The samples were heated in the range 20–1000 °C with a heating rate of 10 °C/min in a He atmosphere.

Major- and trace-element analyses, including the LREE, were obtained by XRF analysis (ARL8420+ WD/XRF spectrometer). The materials were dried at 105 °C, ground in a Tema mill, and passed through a 75 μm sieve. Major elements (Si, Al, Ti, Fe, Mn, Mg, Ca, Na, K, and P) were determined on fused glass disks (Bennett and Oliver 1976, modified by N. Marsh, University of Leicester, U.K.) The samples were fused using a mixture of 80% Li-tetraborate and 20% Li-metaborate as flux. Trace elements (Ba, Ce, Co, Cu, Ga, La, Nb, Nd, Ni, Pb, Rb, Sc, Sr, Th, U, V, Y, Zn, Zr, and S) were determined on pressed powder pellets. Sample preparation methods and analytical precision and accuracy for the instrument and the methods used are given in Christidis (1998).

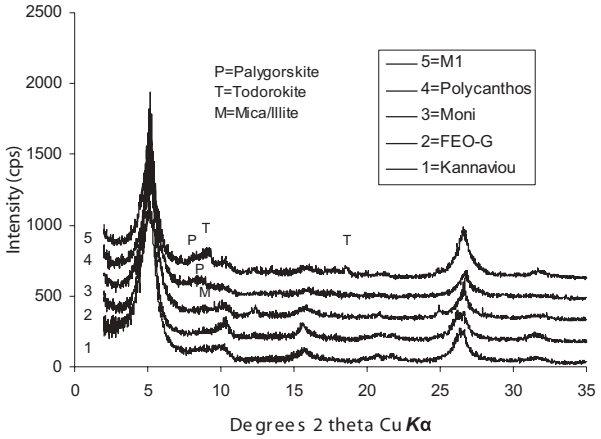

FIGURE 4. XRD traces of oriented clay fractions of the Cyprus bentonites.

RESULTS

Mineralogy and mineral textures

The mineralogical composition of the Cyprus bentonites are listed in Table 1. All samples contain smectite as a major component in variable contents (40–60%). The *b*-parameter of smectite determined from the 060 reflection varies between 8.98 and 9.03, indicating a dioctahedral phase. All deposits contain abundant quartz (10–30%) and plagioclase feldspar (5–20%). Abundant opal-CT and minor illite/mica and kaolinite are present in the deposits of the Polycanthos, the Moni, and the Kannaviou areas. Opal-CT was recognized from the characteristic large diffraction maximum at *d*-values of 4.1 Å followed by a less intense maximum at 4.3 Å (Jones and Segnit 1971). The bentonites at the Polycanthos and Skouriotissa areas contain minor HEU-type zeolite (5–15%), which has the thermal behavior of type III heulandite, i.e., clinoptilolite (Boles 1972). The deposit at the

Kannaviou area contains minor gypsum. Carbonates (calcite, siderite, and dolomite) and chlorite are present in the Polycanthos deposit. SEM revealed the presence of K-rich feldspar, halite, ilmenite, subhedral apatite, a TiO_2 oxide phase, and hematite in most deposits (Fig. 3).

The clay fractions (<2 μm) consist of smectite as the main mineral (Fig. 4). Minor palygorskite is present in all deposits except for the Moni deposit. Minor kaolinite occurs in the Polycanthos and the Moni deposits. Trace illite is present in the FEO-G bentonite and the Moni deposit. Clay-size quartz is also present in minor amounts in all deposits, and opal CT occurs in the Kannaviou and the Polycanthos bentonites. The black horizon of the Polycanthos deposit contains abundant 10 Å Mn oxide, which was identified as todorokite, and trace goethite. The ethylene glycol-saturated smectites display irrationality of the basal reflections spacings. Comparison of the XRD traces with computer-simulated traces using NEWMOD computer code (Reynolds and Reynolds 1996) showed that the XRD traces of most samples can be modeled by assuming an R0 mixed layer illite-smectite with 10–15% illite layers. Moreover, the EDS analyses showed that most samples contain significant amounts of interlayer K. Nevertheless, Ca-saturated ethylene glycol-solvated homoionic samples display well-defined and rational higher order basal reflections. Moreover, with the exception of FEO-G from the Polycanthos deposit, which displays characteristics of group 1a smectites (with $d_{001} \geq 16.6$ Å, and rational higher order basal reflections, i.e., typical low-charge smectites), K-saturated samples display characteristics of group 1b smectites (with 16.6 Å $\geq d_{001} \geq 16$ Å and irrational higher order basal reflections) or even group 2 smectites (with $d_{001} \leq 15$ Å and d_{003} 4.6–4.8 Å, i.e., typical high-charge smectites) (cf. Christidis and Eberl 2003). After back-saturation of the K-saturated samples with Ca and ethylene glycol-solvation, the smectites have rational basal reflections. This fact indicates that those layers, which collapsed after K-saturation, re-expanded fully after subsequent Ca-saturation. Therefore, the irrationality of basal reflections observed in Figure 4 is related to the existence of exchangeable interlayer K in the original smectite.

TABLE 1. Mineral assemblages of the Cyprus bentonites

	Polycanthos	Skouriotissa	Kannaviou	Moni
Smectite	M	M	M	M
Illite/Mica	Min	–	Min	Min
Kaolinite	Min	–	Min	Min
Palygorskite	Min	Min	Min	–
Chlorite	T	–	–	–
Clinoptilolite	Min	Min	–	–
Quartz	M	M	M	M
Opal-CT	M	–	M	M
Plagioclase	Min	Min	Min	Min
K-feldspar	T	T	T	T
Calcite	Min	–	–	–
Dolomite	Min	–	–	–
Siderite	Min	–	–	–
Apatite	T	T	T	T
Gypsum	–	–	Min	–
Hematite	T	T	T	T
Goethite	T	–	–	–
Todorokite	Min	–	–	–
Ilmenite	T	T	T	T
TiO_2	T	T	T	T
Halite	T	T	T	–

Notes: M = major phase, Min = minor phase, T = trace phase.

Under the SEM, smectite forms flat, slightly wavy flakes, commonly elongated (Figs. 5a and 5b). Typical honeycomb textures are not common, which is attributed to compaction of the bentonites during diagenesis and to the chemical characteristics of the smectite. The bentonites contain Fe-rich smectite, which tend to form elongated flakes. Owing to the age of the deposits and the influence of diagenesis, relics of glass shards have not been preserved. In contrast, smectite has replaced radiolarian frustules and plagioclase (Figs. 3a and 5c). Similarly, clinoptilolite forms typical tabular crystals often closely associated with radiolarian frustules (Figs. 5d and 5e). Replacement of radiolarian frustules by smectite and clinoptilolite releases Si, which forms acicular or spherical opal-CT crystals. Such opal-CT textures are common in bentonites (Christidis et al. 1995). In the black horizon of the Polycanthos deposit, acicular crystals of todorokite are present (Fig. 5f) and account for the large amounts of Mn observed (see below). Therefore, even in Mn-rich environments, smectite is not an important host of Mn. Acicular palygorskite crystals are draped over smectite flakes and often form aggregates (Figs. 5f, 5g, and 5h). The palygorskite, which forms crystals thinner, longer and more delicate than todorokite, is Mn-free and has replaced smectite (Figs. 5f, 5g, and 5h). EDS analysis showed an Fe signal in palygorskite. However, owing to the delicate nature of the palygorskite crystals, the Fe-signal probably originates from the smectitic background, rather than from the palygorskite itself.

IR and DTA-TG results

Representative FTIR spectra of smectites from different horizons of the Polycanthos deposit are shown in Figure 6. The spectra are typical for dioctahedral smectites (Madejova and Komadel 2001) and display features that are characteristic of Fe-rich smectites (Bishop et al. 2002). The bands at 3620 cm^{-1} and 3570 cm^{-1} are attributed to Al-OH and Fe-OH stretching, respectively. The band at 3692 cm^{-1} is attributed to minor kaolinite present in the clay fraction. The bands at 915 cm^{-1} and 870 cm^{-1} are attributed to AlAlOH and AlFeOH bending, respectively. Two additional bands are observed at 885 cm^{-1} and 830–835 cm^{-1}. The former is attributed also to AlFeOH bending of a Fe-poorer phase, indicating the presence of two smectites having different Fe-contents. The latter is attributed to FeFeOH bending. Typically this band occurs at ~820 cm^{-1} (Bishop et al. 2002; Gaudin et al. 2004), but after heating, it migrates to 835 cm^{-1} (Köster et al. 1999). Alternatively, this band can be attributed to the presence of an Al-Fe-Mg-bearing mica, which displays a band at ca. 835 cm^{-1} (Odin et al. 1988). Mica with celadonitic composition has been identified in most study areas (see below, also Table 1). Celadonitic mica is a typical alteration product in Troodos pillow lavas (Gillis and Robinson 1990). The band at 695 cm^{-1} is attributed to Fe-O out-of-plane vibrations, whereas those at ca. 520 cm^{-1}, 465–470 cm^{-1}, and 427 cm^{-1} are attributed to Al-O-Si deformation, Si-O-Si deformation, and Si-O bending, respectively (Bishop et al. 2002).

The DTA-TG analysis showed a low temperature of dehydroxylation for smectites at ca. 550 °C, characteristic of "non-ideal" smectites (Schultz 1969). Such dehydroxylation temperatures are typical for *trans*-vacant smectites (Drits et al.

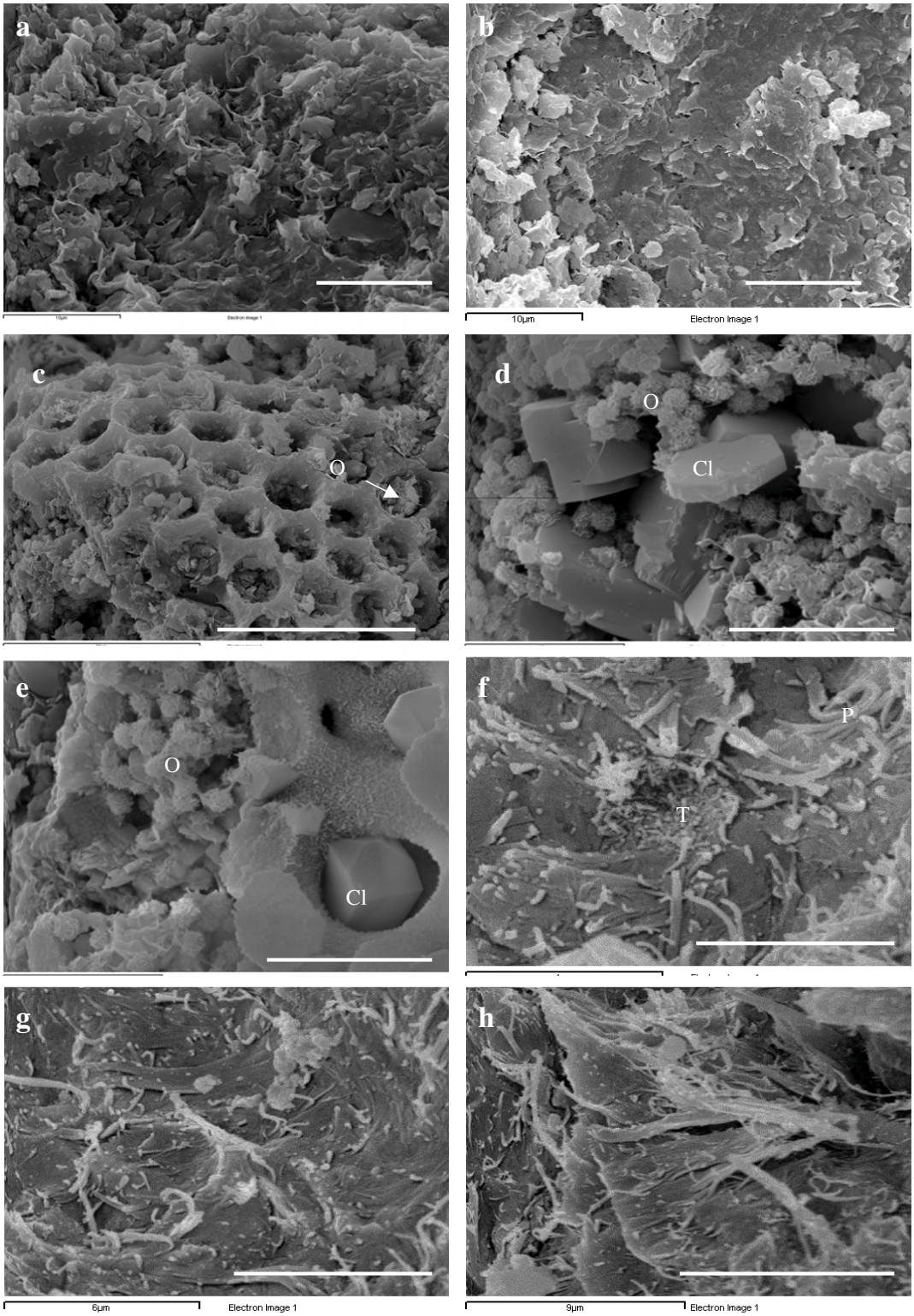

FIGURE 5. SEM photographs of the Cyprus bentonites. (**a**) Wavy smectite flakes showing honeycomb texture. Scale bar = 10 µm. (**b**) Well-compacted smectite flakes with parallel orientation. Scale bar = 10 µm. (**c**) Pseudomorphic replacement of radiolarian frustule by smectite. O = opal-CT. Scale bar = 30 µm. (**d**) Clinoptilolite (Cl) and opal-CT spherules crystals filling voids. Scale bar = 10 µm. (**e**) Clinoptilolite (Cl) crystals growing in voids of radiolarian frustules. O = opal-CT. Scale bar = 10 µm. (**f**) Todorokite (T) crystals and palygorskite replacing smectite. Scale bar = 4 µm. (**g**) Acicular palygorskite crystals replacing smectite. Scale bars = 6 and 9 µm, respectively.

TABLE 2. Microprobe analyses and structural formulae of smectites from the Cyprus bentonites

	Polycanthos deposit																			
	APL (*n*=6)				G7 (*n*=20)				K4 (22)				FEO-G (*n*=9)				M1 (*n*=20)			
	Mean	s.d.	Min.	Max	Mean	s.d.	Min.	Max	Mean	s.d.	Min.	Max	Mean	s.d.	Min.	Max	Mean	s.d.	Min.	Max
SiO_2	56.02	1.87	54.15	58.67	55.65	1.25	53.59	58.17	53.55	4.28	43.61	61.39	60.67	2.05	57.67	63.46	48.58	3.19	44.20	53.94
Al_2O_3	15.60	1.39	14.30	17.91	15.20	2.20	12.36	22.12	15.17	3.18	11.15	23.13	21.05	0.70	20.14	22.06	12.84	1.55	10.57	16.31
Fe_2O_3	9.94	1.91	8.28	12.23	9.01	2.26	4.61	12.36	11.51	3.84	2.41	16.55	0.87	0.22	0.43	1.22	13.30	1.65	9.89	15.58
MgO	3.38	0.13	3.22	3.56	3.38	0.37	2.66	4.06	2.95	0.54	1.67	4.11	3.81	0.25	3.50	4.23	3.44	0.43	2.59	3.96
CaO	0.21	0.21	0	0.50	0.94	0.54	0.42	2.35	0.73	0.43	0	1.52	0.50	0.38	0	1.35	0.75	0.47	0	2.12
Na_2O	0.44	0.31	0	0.86	0.54	0.11	0.43	0.82	0.71	0.20	0.45	1.09	2.24	0.58	1.40	3.35	0.90	0.29	0.60	1.61
K_2O	2.63	0.83	1.71	3.82	1.48	0.90	0.62	4.19	1.88	1.27	0.64	4.74	0	0	0	0	1.90	1.19	0.92	5.22
Total	88.22				86.19				86.49				89.13				81.71			
Structural formulae based on 11 O atoms																				
Tetrahedral Cations																				
Si	3.894	0.065	3.803	3.982	3.929	0.062	3.724	3.994	3.826	0.121	3.563	0.021	3.975	0.009	3.962	3.987	3.739	0.043	3.662	3.835
^{IV}Al	0.106	0.065	0.018	0.197	0.071	0.062	0.006	0.276	0.174	0.121	3.979	0.437	0.025	0.009	0.013	0.038	0.261	0.043	0.165	0.338
Octahedral Cations																				
^{VI}Al	1.173	0.097	1.065	1.281	1.191	0.124	1.045	1.503	1.107	0.201	0.868	1.679	1.598	0.018	1.537	1.630	0.900	0.100	0.733	1.077
Fe^{3+}	0.519	0.097	0.425	0.635	0.478	0.118	0.237	0.662	0.612	0.189	0.141	0.863	0.043	0.011	0.020	0.062	0.772	0.106	0.576	0.929
Mg	0.308	0.020	0.283	0.335	0.331	0.042	0.259	0.422	0.281	0.053	0.180	0.348	0.359	0.020	0.183	0.328	0.328	0.031	0.267	0.406
Interlayer Cations																				
Ca	0.015	0.016	0	0.037	0.071	0.039	0.032	0.171	0.056	0.033	0	0.106	0.035	0.026	0	0.093	0.063	0.040	0	0.176
Mg	0.043	0.027	0.002	0.068	0.024	0.025	0	0.067	0.034	0.034	0	0.088	0.014	0.013	0	0.044	0.069	0.047	0	0.134
Na	0.059	0.043	0	0.120	0.073	0.015	0.057	0.111	0.099	0.030	0.058	0.152	0.284	0.070	0.175	0.409	0.135	0.045	0.091	0.242
K	0.233	0.073	0.151	0.341	0.132	0.078	0.056	0.359	0.173	0.121	0.057	0.470	0	0	0	0	0.184	0.104	0.086	0.475
L Charge	0.414	0.049	0.353	0.480	0.402	0.063	0.317	0.536	0.455	0.082	0.348	0.628	0.384	0.025	0.349	0.421	0.589	0.055	0.479	0.656
Int. Charge	0.408	0.050	0.345	0.475	0.395	0.064	0.310	0.536	0.452	0.082	0.343	0.624	0.382	0.025	0.345	0.417	0.583	0.055	0.473	0.65
Tet. charge	0.256	0.124	0.051	0.410	0.177	0.110	0.018	0.515	0.382	0.193	0.058	0.708	0.065	0.021	0.036	0.094	0.443	0.046	0.331	0.518

TABLE 2.— *Continued*

	Kannaviou deposit								Skouriotissa deposit				Moni deposit							
	BENA (*n*=8)				BENB (*n*=20)				SK (*n*=27)				VB (*n*=28)				VG (*n*=21)			
	Mean	s.d.	Min.	Max	Mean	s.d.	Min.	Max	Mean	s.d.	Min.	Max	Mean	s.d.	Min.	Max	Mean	s.d.	Min.	Max
SiO_2	52.00	2.57	47.13	54.70	53.20	2.14	56.97	49.70	54.01	2.77	15.95	60.32	47.33	5.09	42.69	58.49	50.63	3.93	43.49	58.27
Al_2O_3	13.39	1.55	11.34	15.88	13.21	1.51	16.23	10.31	15.16	1.32	13.26	19.58	16.02	2.56	11.65	22.23	16.67	3.66	13.24	25.91
Fe_2O_3	10.70	3.24	7.20	15.32	10.79	2.81	14.72	5.52	10.30	2.00	5.88	14.08	9.31	2.61	4.89	15.76	9.68	3.08	3.15	15.78
MgO	3.22	0.49	2.47	3.98	3.49	0.54	4.75	2.52	3.81	0.49	2.63	4.67	2.12	0.50	1.30	3.11	2.69	0.69	1.30	3.92
CaO	0.20	0.39	0	1.01	0.44	0.33	1.01	0	0.54	0.17	0	0.76	0.65	0.22	0	1.09	0.85	0.31	0.36	1.68
Na_2O	1.63	0.85	0.76	3.19	1.29	0.78	3.10	0.28	0.57	0.41	0.19	1.97	0.45	0.48	0	1.96	0.60	0.10	0.42	0.76
K_2O	2.01	1.07	0.65	3.50	2.09	1.01	4.17	0.48	1.78	0.91	0.44	5.13	1.54	0.75	0.38	3.76	1.52	0.62	0.78	3.39
Total	83.14				84.51				86.16				77.41				82.64			
Structural formulae based on 11 O atoms																				
Tetrahedral Cations																				
Si	3.877	0.113	3.641	3.969	3.898	0.077	3.688	3.995	3.847	0.081	3.696	3.980	3.748	0.123	3.535	3.991	3.763	0.129	3.374	3.972
^{IV}Al	0.123	0.113	0.031	0.359	0.102	0.077	0.005	0.312	0.153	0.081	0.02	0.304	0.252	0.123	0.009	0.465	0.237	0.129	0.028	0.626
Octahedral Cations																				
^{VI}Al	1.051	0.120	0.850	1.225	1.039	0.128	0.790	1.302	1.123	0.105	0.909	1.388	1.247	0.173	0.984	1.577	1.219	0.184	0.929	1.737
Fe^{3+}	0.597	0.166	0.393	0.839	0.591	0.154	0.308	0.834	0.551	0.102	0.324	0.781	0.554	0.142	0.298	0.822	0.535	0.139	0.168	0.774
Mg	0.352	0.061	0.263	0.436	0.370	0.051	0.291	0.494	0.326	0.033	0.267	0.388	0.199	0.067	0.038	0.329	0.246	0.097	0	0.368
Interlayer Cations																				
Ca	0.016	0.031	0	0.079	0.034	0.025	0	0.081	0.041	0.013	0	0.059	0.056	0.020	0	0.098	0.069	0.028	0.027	0.153
Mg	0.006	0.028	0	0.047	0.010	0.030	0	0.118	0.076	0.036	0	0.141	0.053	0.040	0	0.157	0.054	0.047	0	0.164
Na	0.238	0.127	0.105	0.450	0.184	0.111	0.039	0.453	0.078	0.055	0.027	0.266	0.070	0.073	0	0.302	0.088	0.017	0.055	0.114
K	0.189	0.095	0.060	0.319	0.195	0.093	0.046	0.371	0.163	0.089	0.039	0.480	0.158	0.073	0.039	0.424	0.144	0.058	0.072	0.307
L Charge	0.475	0.088	0.380	0.635	0.472	0.056	0.404	0.615	0.479	0.068	0.369	0.638	0.451	0.110	0.260	0.632	0.484	0.073	0.315	0.616
Int. Charge	0.471	0.087	0.375	0.630	0.467	0.055	0.402	0.606	0.475	0.068	0.362	0.631	0.446	0.109	0.259	0.623	0.477	0.073	0.307	0.607
Tet. Charge	0.258	0.177	0.075	0.565	0.216	0.136	0.012	0.507	0.319	0.132	0.050	0.524	0.559	0.205	0.034	0.91	0.489	0.215	0.089	0.940

Notes: Exchangeable Mg was calculated by difference from total Mg assuming the total number of octahedral cations is 2.00 phfu. s.d.= standard deviation, min= minimum value, max= maximum value. L Charge= Layer Charge, Int. Charge= Interlayer Charge, Tet. Charge = proportion of tetrahedral charge.

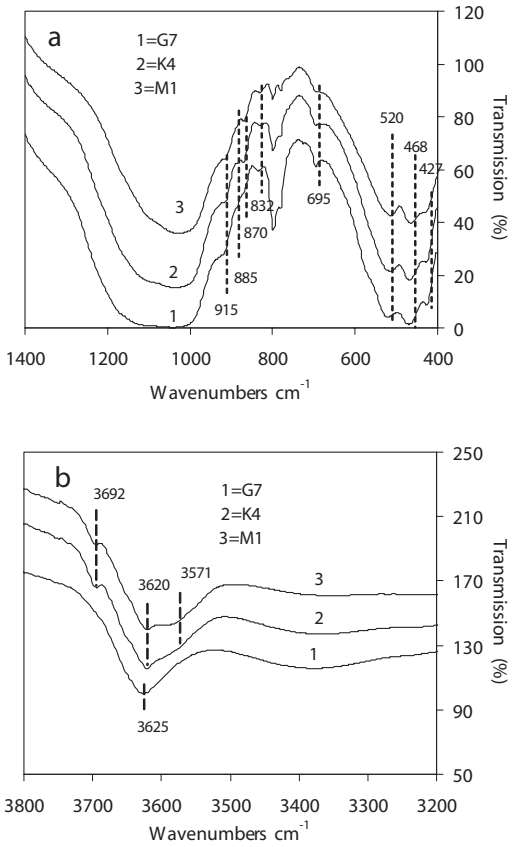

FIGURE 6. FTIR spectra of representative clay fractions form the Polycanthos deposit. (**a**) Lattice vibrations, (**b**) OH-stretching vibrations. M1 = black horizon (umber), G7 = Green bentonite, and K4 = brown bentonite.

1998). The smectite from the black horizon of the Polycanthos deposit, which has a slightly lower dehydroxylation temperature, has the highest octahedral Fe content (see below). Nevertheless there is no systematic correlation between the dehydroxylation temperature and octahedral Fe content. The smectite from the FEO-G bentonite has a high dehydroxylation temperature at 690 °C typical of *cis*-vacant smectites. Therefore, the FTIR and DTA data and the smectite morphology observed in the SEM, indicate that the Cyprus smectites are Fe-rich.

Smectite chemistry

Average values of the elements analyzed and the cation distributions, standard deviations, and minimum and maximum values are listed in Table 2. The smectite, except that from sample FEO-G, which is homogeneous, displays considerable compositional variation similar to its counterparts derived from acidic and intermediate rocks (Christidis and Dunham 1993, 1997), although it has considerably different composition. The smectite has layer charges that vary between –0.25 and –0.65 per half formula unit (phfu). In most samples, a few analyses yielded a layer charge between –0.75 phfu and –0.88 phfu and a moderate K-content (0.25–0.50 atoms phfu) suggesting the existence of a mica component with mixed celadonitic-glau-

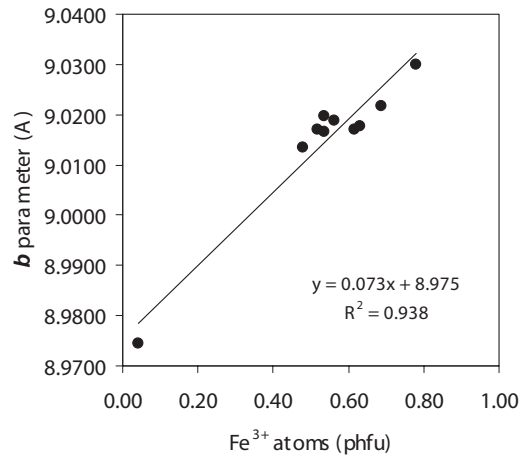

FIGURE 7. Relationship between Fe^{3+} and *b* parameter of smectite. The corresponding empirical regression equation is: *b* (Å) = 8.975 + 0.074 Fe^{VI} ± 0.0039.

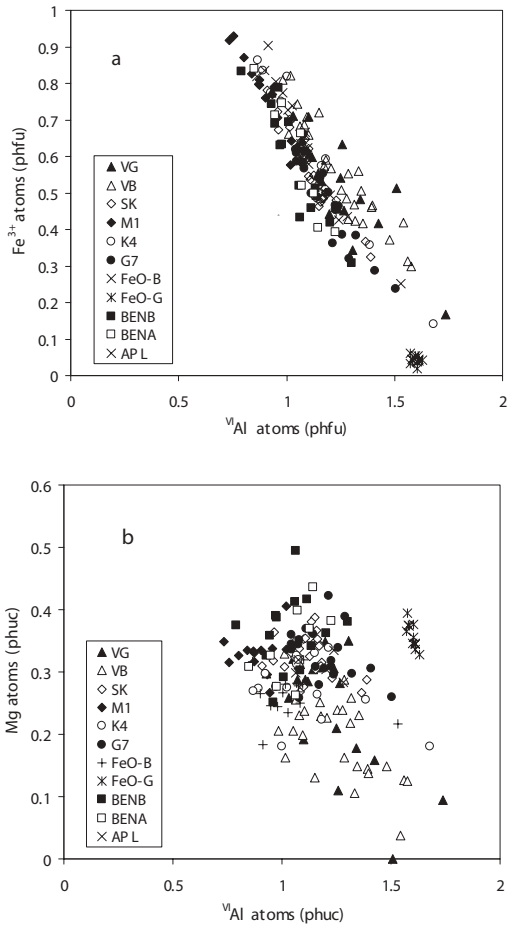

FIGURE 8. Plots of (**a**) ^{VI}Al vs. $^{VI}Fe^{3+}$ and (**b**) ^{VI}Al vs. ^{VI}Mg in Cyprus smectites. See text for discussion. Key to the sample codes: APL, FEO-B, FEO-G, K4, and G7, Polykanthos deposit, M1 = black horizon (umber), Polykanthos deposit, BENA, BENB Kannaviou deposit, SK = Skouriotissa deposit, VB, VG = Moni deposit.

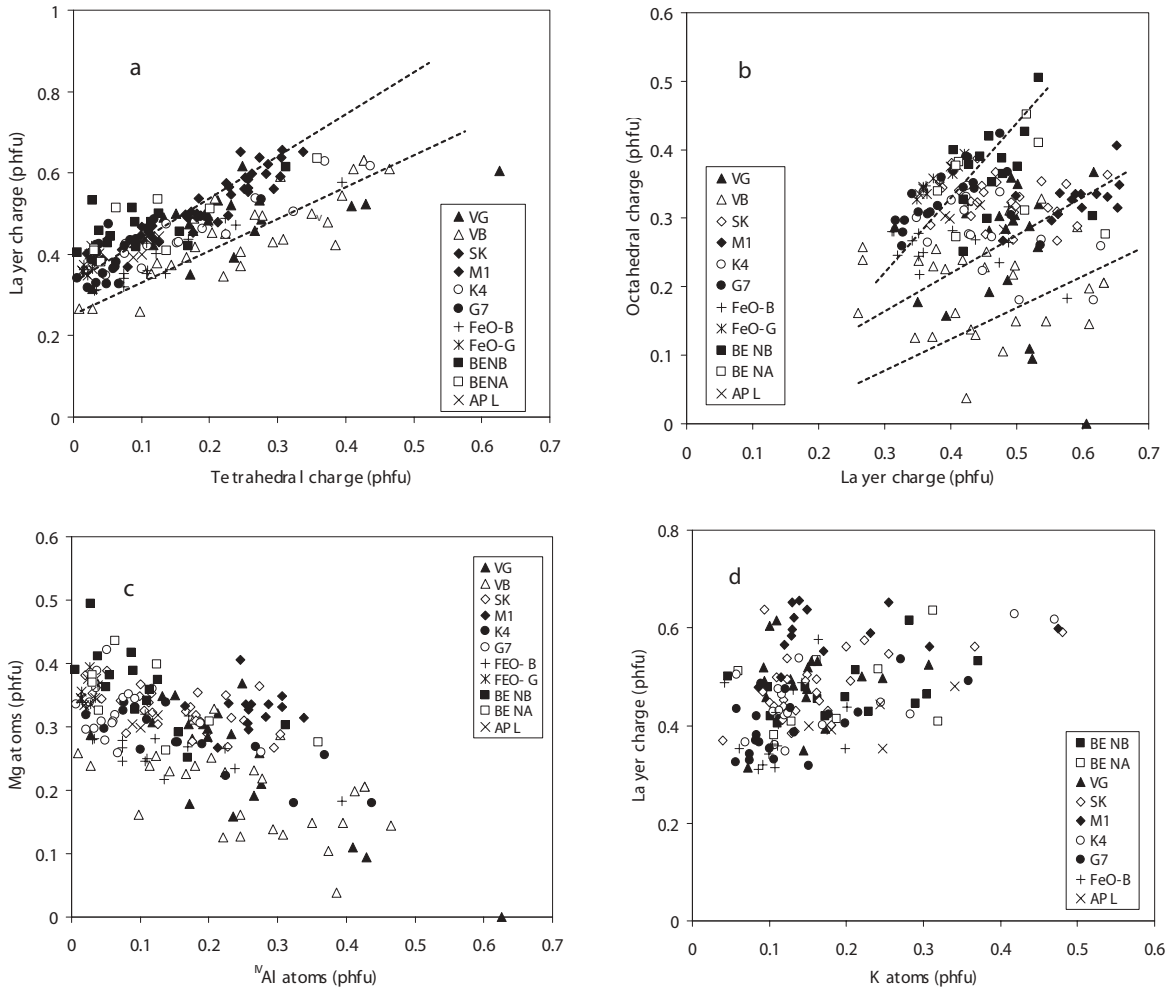

FIGURE 9. Plots showing the relationship between (**a**) total layer charge and tetrahedral layer charge, (**b**) total layer charge and octahedral layer charge, (**c**) octahedral Mg and tetrahedral layer charge, and (**d**) K and tetrahedral layer charge of Cyprus smectite. The dashed lines indicate schematically the different trends observed in Cyprus smectite. Labels as in Figure 8.

conitic composition. These analyses were not considered for further study. All smectites, except those from sample FEO-G, have high-octahedral Fe contents. Moreover, in several bentonites, the smectite has a considerable tetrahedral charge. In general, the smectite from the Moni deposit has greater tetrahedral charge and lower Mg content than its counterparts from the other deposits. Nevertheless, with the exception of smectite from sample VB, which is beidellite, the tetrahedral charge in the remaining smectite phases does not exceed 50% of the total charge, suggesting that the smectite is Fe-rich montmorillonite. The possibility for contamination of Fe from amorphous Fe oxides was tested by projection of octahedral Fe vs. the *b* cell parameter obtained from the 060 diffraction maximum (Fig. 7). A well-expressed positive linear relationship was observed with correlation coefficient (r) 0.969.

The *b* cell parameters calculated from the regression equation for Fe-smectites are similar to those obtained by Russell and Clarke (1978) but larger than those obtained by Brigatti (1983) for Fe-rich smectites derived from the weathering of basaltic rocks. The observed difference is attributed to the fact that smectites of this study have Fe contents close to or lower than the lower limit for which the linear equation of Brigatti is valid. Indeed, Brigatti (1983) suggested that smectite containing less than 0.5–0.6 Fe^{3+} atoms phfu may not follow the regression equation she calculated.

Smectite from sample FEO-G has different crystal-chemical characteristics. This smectite is nearly ideal montmorillonite with negligible tetrahedral charge (i.e., in this respect it is similar to Otay-type montmorillonite), and it does not contain exchangeable K. However, it has too low a layer charge (less than –0.40 phfu) for Otay-type montmorillonite (cf. Newman and Brown 1987). Such a layer charge is typical for Wyoming-type montmorillonite. However, unlike its Wyoming counterparts, the FEO-G montmorillonite is Fe-poor containing <0.1 Fe-atoms phfu. Smectite with such chemical features (i.e., negligible tetrahedral charge, low layer charge, and low Fe content) is not believed to have been reported previously. According to its crystal-chemical features, it can be characterized as low-charge

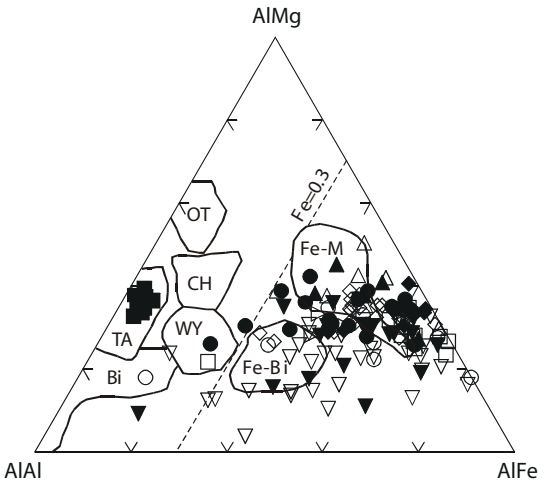

FIGURE 10. Ternary plot (after Güven 1988) of Cyprus smectite compositions. Key to the abbreviations. OT = Otay-type montmorillonite, TA = Tatatilla-type montmorillonite, CH = Chambers-type montmorillonite, WY = Wyoming-type montmorillonite, Bi = Beidellite, Fe-Bi = Fe-rich beidelite, and Fe-M = Fe-rich montmorillonite.

Otay-type montmorillonite.

The relationships between the octahedral cations of Cyprus smectite are shown in Figure 8. A well-expressed negative trend occurs between Fe^{3+} and ^{VI}Al. The relationship is general and describes the total population, including the Fe-poor smectite from sample FEO-G (Fig. 8a). A negative relationship, although not well expressed, is observed also between ^{VI}Al and Mg (Fig. 8b). The smectite from sample FEO-G does not follow the trend. No particular trend occurs between Fe^{3+} and Mg. Therefore, the relative abundance of Fe and to a lesser degree of Mg, are the main factors controlling the systematic compositional variations of the Cyprus smectite.

A well-expressed positive trend occurs between total layer charge and tetrahedral charge (Fig. 9a). Smectite of sample VB from the Moni area deviates from the overall trend, although it is characterized by a similar relationship. In contrast, the relationship between total layer charge and octahedral charge is not very clear, and considerable scatter in the data is observed. This scatter leads to three possible trends (dashed lines in Fig. 9b). It follows that variations in total layer charge are controlled mainly by variations in the tetrahedral charge. Also, a negative trend holds between tetrahedral charge and octahedral Mg (Fig. 9c). Finally, a positive relationship holds between exchangeable K and total layer charge (Fig. 9d), although there is considerable scatter. In the latter diagram, samples VB and FEO-G deviate from the overall trend and are not plotted. The former does not display any obvious trend between K and total layer charge and the latter is K-free.

In the diagram proposed by Güven (1988), the smectites plot in and close to the "fields" of Fe-montmorillonite and, to a lesser degree, of Fe-rich beidellite (Fig. 10). A few analyses plot as Wyoming montmorillonite and normal beidellite. Such compositions are typical of soil smectite derived from weathering of basaltic and/or ultrabasic rocks rocks (Brigatti 1983; Gaudin et al. 2004) and less often smectite from bentonites (English Fullers' earths, Grim and Güven 1978; Czech bentonites, Cicel et al. 1992). Smectite from the Moni area (sample VB) contains less octahedral Mg than smectite from other areas and plots in the "field" of Fe-beidellite, in accordance with their chemical composition (Table 2). However, most smectite analyses from sample VG plot as Fe-montmorillonite, although the average tetrahedral charge for these smectites is 49% of the total layer charge, i.e at the boundary montmorillonite-beidellite (Table 2). Smectites from sample FEO-G have different chemical characteristics and plot in the field of Tatatilla-type montmorillonite, although these smectites have a considerably smaller layer charge and very low tetrahedral charge compared to the typical Tatatilla-type montmorillonite (Newman and Brown 1987).

Chemistry of the bentonites

Representative bulk-rock analyses of the Cyprus bentonites are listed in Table 3. The bentonites display similar bulk-rock chemical characteristics, although they come from different areas. They are characterized by high Fe_2O_3, low Al_2O_3, moderate TiO_2, and variable SiO_2. Also, they have relatively high K_2O compared with most common bentonites, but their Na_2O and CaO contents are typical of bentonites (cf. Grim and Güven 1978). The FEO-G bentonite (analysis 3) from the Polycanthos deposit has a different chemical composition characterized by low Fe_2O_3, high Al_2O_3, and low K_2O and TiO_2 contents. Samples M1 and M2 from the black horizon (umber) of the Polycanthos deposit have high MnO and higher K_2O than the remaining bentonites (analyses 10 and 11). Although the SiO_2/Al_2O_3 ratio of the bentonites varies between broad limits, the Al_2O_3/Fe_2O_3 ratio is rather constant close to 2. The Fe-poor FEO-G bentonite has a very high Al_2O_3/Fe_2O_3 ratio and samples from the black horizon of the Polycanthos deposit have lower Al_2O_3/Fe_2O_3 ratios (Table 3).

The distribution of main chemical elements between smectite and bulk rock is depicted in the elemental distribution diagrams of Figure 11. In these plots, elemental concentrations have been recalculated on an anhydrous basis. Aluminum, Fe, and Mg are enriched in smectite, relative to the parent rock because they are present mainly in the octahedral sheet of smectite. Silicon, Na, and Ca are enriched in the bulk rock relative to the smectite because they occur in minerals other than smectite that are abundant in the bentonites. These minerals include Si-polymorphs and plagioclase. Finally, K is evenly distributed between smectite and the bulk rock, suggesting that additional K-rich phases are present in the bentonites. At least three K-bearing phases have been recognized in the Cyprus bentonites, namely illite/mica, K-rich feldspar, and clinoptilolite.

Except for the FEO-G bentonite, all materials have Ni, V, Co, and Th contents that are indicative of intermediate-basic precursors (Table 3). These trace elements, which tend to be relatively immobile during alteration, can provide information about the chemical affinity of the parent rocks (Christidis 1998). FEO-G bentonite has low Ni, V, and Co, but a high Th indicative of a different precursor with more acidic affinities. The compatible elements are correlated positively with Fe_2O_3 (Fig. 12a), but inversely with SiO_2 (Fig. 12b). Also, Rb displays a positive correlation with K, which reflects the similar geochemical behavior of the two elements (Fig. 12c).

The LREE are positively correlated with P_2O_5 (Fig. 13), suggesting that they are associated with apatite, the presence of

TABLE 3. Chemical composition of the Cyprus bentonites

	Polycanthos											SK		Kannaviou	Moni	
	1	2	3	4	5	6	7	8	9	10	11	12	13	14	15	16
SiO_2	73.20	64.42	59.54	60.69	66.60	64.02	62.82	68.82	58.66	53.97	53.20	60.40	71.52	69.51	63.49	65.11
TiO_2	0.59	0.75	0.19	0.59	0.60	0.55	0.54	0.55	0.72	0.55	0.74	0.85	0.63	0.67	1.21	1.06
Al_2O_3	10.12	13.36	22.21	16.38	14.06	13.38	14.42	12.00	16.56	15.28	14.37	15.91	10.57	11.43	14.75	14.47
Fe_2O_3	4.56	7.84	3.20	5.71	6.58	7.30	7.14	6.90	8.55	11.04	11.05	7.08	5.51	5.75	7.05	6.29
MnO	0.06	0.09	0.08	0.15	0.07	0.18	0.10	0.12	0.17	3.03	3.26	0.16	0.14	0.13	0.11	0.10
MgO	2.20	3.16	3.68	4.06	3.08	2.81	2.54	2.44	3.41	3.44	3.88	3.92	2.47	2.70	2.30	2.65
CaO	0.95	1.00	0.98	1.12	0.94	1.17	1.02	1.15	1.27	1.22	1.48	1.20	0.97	0.98	1.65	1.21
Na_2O	0.97	1.13	1.52	1.54	0.72	1.56	1.79	1.27	1.66	1.19	1.22	1.66	1.48	1.58	0.60	0.70
K_2O	1.52	1.62	0.55	1.95	1.40	1.83	2.59	1.83	2.26	2.84	2.59	2.37	1.49	1.66	2.19	1.94
P_2O_5	0.36	0.42	0.09	0.19	0.31	0.39	0.27	0.35	0.15	0.51	0.50	0.25	0.20	0.22	0.20	0.22
LOI	4.50	5.55	6.89	7.03	5.43	6.35	6.88	5.13	6.78	6.42	6.90	6.21	4.24	4.60	5.87	5.54
Total	99.03	99.34	98.93	99.41	99.79	99.53	100.11	99.88	100.19	99.49	99.19	100.01	99.22	99.23	99.42	99.29
S/A	7.23	4.82	2.68	3.70	4.74	4.78	4.36	5.68	3.54	3.53	3.70	3.80	6.77	6.08	4.30	4.50
A/F	2.22	1.70	6.94	2.87	2.14	1.83	2.02	1.74	1.94	1.38	1.30	2.25	1.92	1.99	2.09	2.30
Trace elements																
Ba	91.5	115.6	243.5	447.8	268.7	252.9	358.3	279.4	179.1	716.5	393.5	165.1	111.2	130.8	160.8	131.5
Ce	46.6	73.6	10.6	83	95	133	112	108	104	213	163.1	62	47.9	53	64.4	61.4
Co	18.5	29.5	13	22	28	34	31	29	48	59	58.3	29.4	20.6	19	22.2	20.1
Cu	41.6	107.9	349.9	180	97	201	105	79	78	200	198.6	105.2	54.5	77.4	84	149.6
Ga	11.7	15.6	22.4	13	10	13	13	11	16	13	16	18.2	14.1	13.8	18.3	17.3
La	32.1	41	6.2	39	33	63	48	53	40	90	81.1	31.5	23	27	34.9	33.2
Nb	10.3	12.5	12.2	13	14	19	21	18	20	21	12.4	12.4	13.2	12.5	24.9	20.1
Nd	29.1	38.1	8	25	23	43	37	36	36	84	75.6	30	23.2	25.3	32.9	31.3
Ni	54	87.7	66.3	79	90	106	91	67	138	171	223.2	99.9	66.3	51.8	62	59.2
Pb	13.3	10.1	10.2	24	0	10	20	9	24	107	145.1	41.6	15	18.4	15.9	22
Rb	48.4	60.2	13.5	40	35	47	64	43	59	79	86.8	73.8	52.7	55.3	75.4	64.4
Sc	14.3	18.8	2.1	16.6	18.2	18.1	15.8	17.3	15.1	21.8	23.4	24.8	15.3	17.7	18	19.8
Sr	309.4	151.8	172.4	177	101	240	340	217	289	141	155.8	293.4	186.8	218.3	100.3	111.9
Th	7.2	10.7	60.2	8.4	7.6	8.2	7.8	8.4	7.2	12.9	13.8	10.1	8.2	6.7	13.1	10.5
U	0.9	1.6	0.3	0.7	0.8	1.0	0.8	0.9	0.8	1.0	1.1	1.4	0.8	1.1	0.9	1.2
V	98.2	110.9	17	104	68	69	118	63	130	170	267.4	153.6	105.8	123.6	142.2	150.8
Y	39.7	51.8	6	14	14	26	28	23	19	49	85.8	36.6	32.5	36.1	32.9	33.8
Zn	67.1	110.7	142	87	87	104	120	93	131	138	156.7	119.4	56	56.2	79.9	149.8
Zr	90.4	114.7	257.5	86	73	90	94	79	93	125	123.8	118.2	102.5	90.9	211.2	186.5
S	0	617	75	492	407	276	313	291	302	238	183	202	432	402	13182	6894

Notes: Concentrations of major elements are in wt% and of trace elements in ppm. SK = Skouriotissa. S/A = SiO_2/Al_2O_3 ratio, A/F = Al_2O_3/Fe_2O_3 ratio.

which was confirmed by SEM (Fig. 3a). This mineral is commonly observed in bentonites formed at the expense of acidic and intermediate rocks and explains the immobility of LREE relative to HREE in several natural systems (Christidis 1998). Sample FEO-G is characterized by significantly lower LREE concentrations (Table 3).

In the discrimination diagram of Winchester and Floyd (1977), the Cyprus bentonites plot in the fields of andesite/basalt and alkaline basalt (Fig. 14). The FEO-G bentonite plots in the field of trachyte, confirming the significantly different mineralogical and geochemical properties of that material. A basaltic composition is compatible with the geological environment dictated by the Troodos ophiolitic complex. Note that the bentonite data points are aligned parallel to the Nb/Y axis, which denotes the alkaline character of the precursor rocks and that their Zr/TiO_2 ratios, which are indicative of the basic or acid character of the precursor rocks, are virtually constant. Formation of bentonites is usually associated with a preferential leaching of Y yielding an artificial increase of the Nb/Y ratio, whereas both Zr and Ti are essentially immobile during bentonite formation, even at very intensive alteration (Christidis 1998). The highly variable Nb/Y ratio suggests that release of Y may well have occurred during alteration of the precursor glass. This is the case especially for the FEO-G bentonite, which certainly displays alkaline affinities.

DISCUSSION

Precursors of the Cyprus bentonites

Notwithstanding the lack of fresh volcanic shards and/or the existence of pseudomorphic replacement textures of glass shards by smectite often present in bentonites (e.g., Khoury and Eberl 1982; Christidis 2001), there are certain characteristics that indicate a volcanic nature for the parent rocks of the Cyprus bentonites. These characteristics include (1) the stratigraphic position of the bentonites and their geological relationship with the underlying Upper Pillow lavas of the Troodos ophiolitic suite; (2) the trace-element compositions of the bentonites, which indicate an igneous signature; and (3) the presence of characteristic phases of igneous origin such as apatite, intermediate plagioclase, and mixed Na,K (alkali) feldspar. Although the relatively small number of samples does not allow a reliable multivariate statistical analysis, it seems that with one exception (sample FEO-G), the bentonites probably were derived from a common precursor and that the variable physical properties of the bentonites (e.g., the rheological and swelling properties) may be related to the smectite crystal-chemical characteristics and the variable concentration of non-smectitic minerals, especially Si-polymorphs.

The discrimination diagram of Winchester and Floyd (1977) (Fig. 14) suggests that the parent rocks of most of the Cyprus

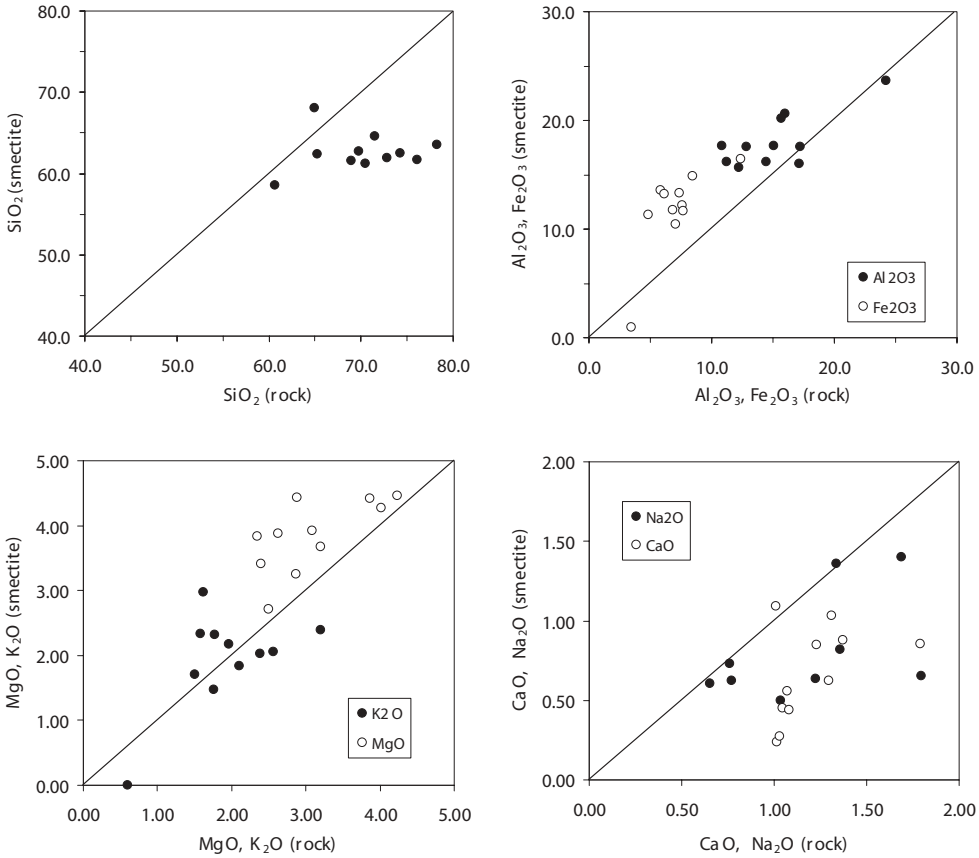

FIGURE 11. Diagrams comparing the concentrations (in wt% oxide) of major elements in Cyprus smectite and bentonites.

bentonites had intermediate-basic composition, being possibly andesites or basaltic andesites. Although the observed shift toward the alkaline basalt field can be attributed to preferential leaching of Y relative to Nb during alteration, the observed Zr/TiO_2 ratios are reliable indictors of the basicity of the precursor rocks (Christidis 1998). The different parent composition of FEO-G suggests that the character of volcanism has changed with time and that, at short intervals, more acidic rocks were erupted from the spreading center. However, the pronounced alkaline signature of this sample is also compatible with preferential depletion of Y during bentonite formation. The eruption of more acidic volcanic rocks is compatible with the suprasubduction geotectonic setting of the Troodos complex, in which contamination with crustal material is common. Such a geotectonic setting is compatible with the formation of water-rich magmas with calc-alkaline character, such as those observed in places in Troodos (Thy 1987), and can explain the eruption of large volumes of pyroclastic materials, the precursors of bentonites, above the higher horizons of the Troodos ophiolite suite.

The basic composition of the parent rocks is at odds with the high SiO_2 contents observed in most samples, because they are typical of bentonites derived from rhyolitic-rhyodacitic rocks (Table 3). Moreover, most samples contain abundant SiO_2 polymorphs, either quartz or opal-CT. Also, the bentonites from Polycanthos and Skouriotissa areas contain minor clinoptilolite, a Si-rich zeolite, whereas basic rocks in the ocean floor usually alter to zeolites, which have low Si/Al ratios, such as phillipsite chabazite or analcime (Hay and Sheppard 2001). Note that the underlying Upper Pillow Lavas, which were affected by hydrothermal metamorphism characterized by zeolitic alteration, contain Si-poor, Al-rich zeolites such as phillipsite, analcime, chabazite, gmelinite, and natrolite, along with saponite, and lesser amounts of clinoptilolite and mordenite (Gillis and Robinson 1990). The high Si contents required for the formation of SiO_2 polymorphs and Si-rich zeolites are explained by the presence of radiolarian frustules, which are abundant in the Cyprus bentonites (Fig. 5). Dissolution of radiolarian frustules and/or their replacement by smectite released Si, which formed either opal-CT or clinoptilolite depending on the microenvironmental pore water chemistry (Fig. 5). Thus, the SiO_2 polymorphs are biogenic in origin. Also, in places, smectite was unstable owing to the high Si-activity of pore waters and was replaced by palygorskite. Formation of palygorskite may well be a later event, because its formation in the underlying pillow lavas has been related to the uplift and emplacement of Troodos during the Miocene (Gillis and Robinson 1990; Staudigel and Gillis 1991). Dissolution was facilitated by the increased heat flow of the ocean floor and the circulation of warm, seawater derived, hydrothermal fluids within the pyroclastic precursors. Thus the high Si activity in the pore water prevented the formation of

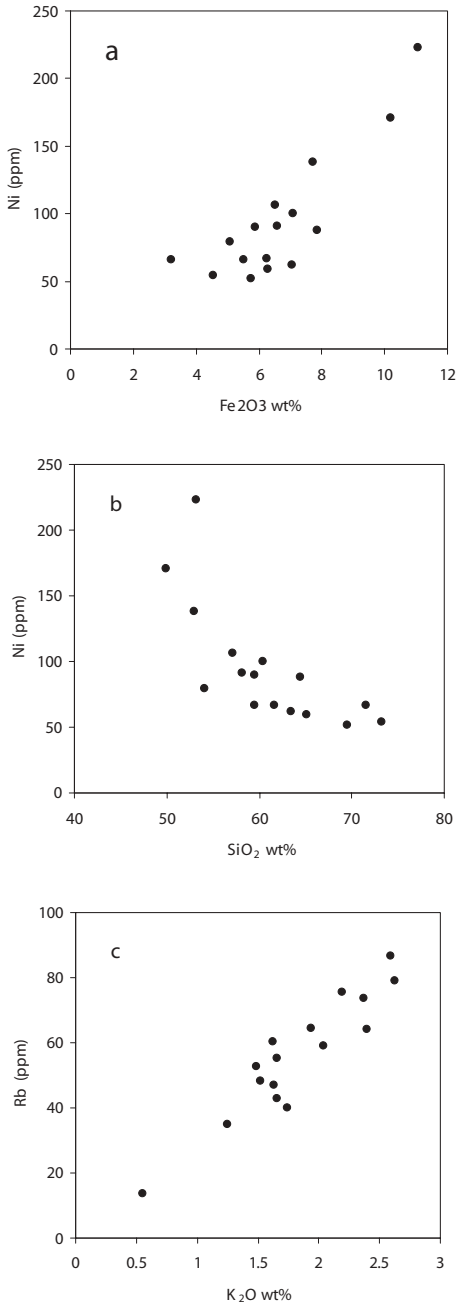

FIGURE 12. Plots of (**a**) wt% Fe_2O_3 vs. ppm Ni, (**b**) wt% SiO_2 vs. ppm Ni, and (**c**) wt% K_2O vs. ppm Rb in the Cyprus bentonites.

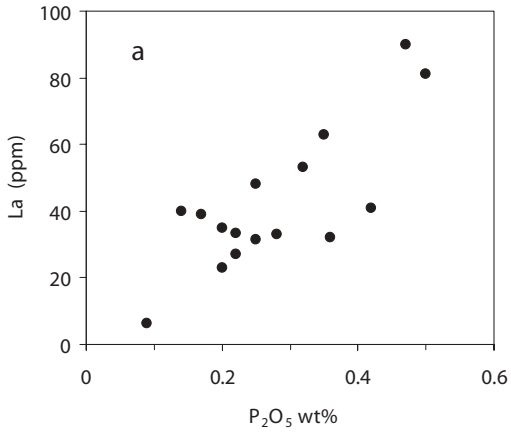

FIGURE 13. Plot of wt% P_2O_5 vs. ppm La in the Cyprus bentonites.

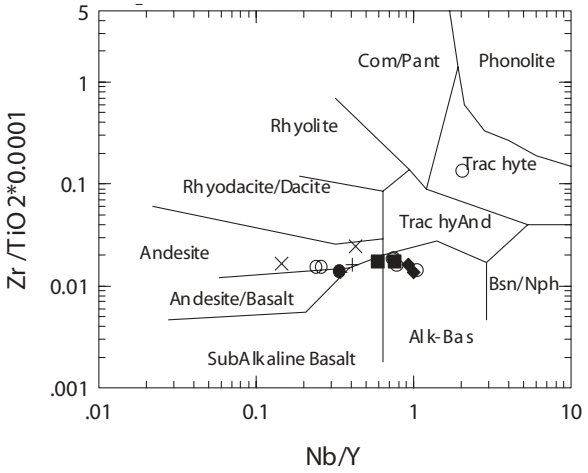

FIGURE 14. Compositions of the Cyprus bentonites plotted in the discrimination diagram of Winchester and Floyd (1977). Key to the symbols: Open circles = brown and grey horizons, diamonds = green horizons and X = black horizons (umber) Polykanthos deposit, full circles = Skouriotissa deposit, + = Kannaviou deposit, full squares = Moni deposit.

zeolites with low Si/Al ratios such as phillipsite and/or chabazite. The relative abundance of biogenic Si is responsible for the great variability in the SiO_2/Al_2O_3 ratio of the bentonites, whereas the Al_2O_3/Fe_2O_3 ratio is essentially constant because both elements are essentially immobile during alteration.

A basic composition of the precursor volcanic rocks is in accordance with the high Fe-content of the bentonites. Nevertheless, this composition cannot account for the high K_2O contents observed in all deposits, a significant part of which is associated with smectite. The high-K contents of bentonites are attributed to low-temperature, seawater-based, circulating hydrothermal waters, heated by the underlying volcanic rocks of the Troodos complex in the ocean floor (Spooner et al. 1977; Gillis and Robinson 1990). For instance, the bentonite in Skouriotissa overlies an extensive Cyprus-type, massive sulfide Cu deposit, which is currently being exploited. In this context, bentonite formation may well represent the lowest temperature alteration event of the Troodos complex, following the higher alteration zone in Upper Pillow Lavas (seafloor weathering zone), which formed at low temperatures as the oceanic crust moved off-axis (Gillis and Robinson 1990). Based on stable isotopes, Köster et al. (1999) showed that a wide range of oceanic and continental Fe-rich smectites, including nontronites, have formed at temperatures below 70 °C. Similar temperatures were adopted by Gillis and Robinson (1990) for the seafloor weathering zone, which contains saponite, and seem reasonable for the smectites studied. The formation of Mn-Fe-rich horizons, known as umbers, under,

or/and within the bentonites (Figs. 1 and 2) via hydrothermal activity and the positive correlation between exchangeable K and layer charge (Fig. 9d) are in accordance with formation of smectite by low-temperature alteration of basic pyroclastics by heated seawater. These horizons have a higher K_2O content on average than the remaining bentonites (Table 3). Alternatively, the alteration processes related to bentonitization, may lead to preferential leaching of Na relative to K during alteration of glass (Shiraki and Iiyama 1990), thus raising the K/Na ratio of the pore fluids and subsequently yielding smectite with interlayer K (Christidis 2001). Smectite formed on the ocean floor during palagonitization is usually K-rich (Zhou and Fyfe 1989). However, although the latter process has been observed in several bentonites associated with alteration of pyroclastic rocks by seawater (Christidis 2001; Matsuda et al. 1996), it does not seem important in the Cyprus bentonites.

Compositional characteristics of smectites: implications for smectite formation

The wide variation in smectite composition of adjacent crystals confirms previous reports for heterogeneity of smectites in bentonites (Christidis and Dunham 1993, 1997; Ddani et al. 2005). In accord with these studies, the source for this heterogeneity is located in: (1) the proportion of tetrahedral charge relative to octahedral charge (i.e., proportion of beidellite vs. montmorillonite component); (2) the variable substitutions in octahedral positions; (3) the relative abundances of the exchangeable cations; and (4) the variation of the total layer charge (Table 2). Sample FEO-G is the only exception to the observed trend because it displays a remarkably homogeneous composition and lack of exchangeable K. The variable chemistry of the octahedral sheet raises the question of solid solution between the various types of smectite, especially between beidellite and Fe-montmorillonite. With the existing data, a solid solution between Fe-rich montmorillonite and Fe-rich beidellite is by no means certain owing to the limitations of the analytical technique used (spot size vs. loss of chemical elements). Under the analytical conditions used, each analytical spot consists on average of ca. 2000 smectite crystallites. Thus, the observed heterogeneity may be attributed to mechanical mixtures of end-member compositions. However, the remarkable homogeneity of smectites in sample FEO-G suggests that even if mechanical mixing exists in the remaining samples, then there must be many "end-member compositions" to explain the pronounced heterogeneity of smectites in those samples. Therefore the observed chemical heterogeneity is considered real. This conclusion, in turn, indicates the significance of microenvironmental conditions during smectite formation and raises the question of whether smectite is indeed a thermodynamically unique phase (Lippmann 1982; May et al. 1986).

Smectite composition in Cyprus bentonites is controlled by the substitution of Fe for Al and to a lesser degree by the substitution of Mg for Al in the octahedral sheet (Fig. 8). A similar relationship holds also for smectite derived from intermediate rocks (Christidis and Dunham 1993), but it is not important in smectite derived from acidic rocks, owing to the lack of Fe (Christidis and Dunham 1997). Thus, the abundance of Fe is more important than Mg for the chemical variability of this smectite, although the parent rocks are expected to contain abundant MgO, in excess of 10%. This fact indicates that Mg was leached during alteration. Therefore, formation of bentonites from basic pyroclastic rocks is associated with significant depletion of Mg, opposite to their counterparts from acidic and, to a lesser degree, from intermediate pyroclastic rocks. Note that hydrothermal alteration of the underlying pillow lavas yielded saponite, Fe-rich in places, instead of ferruginous montmorillonite (Gillis and Robinson 1990). The saponite has an intermediate dioctahedral-trioctahedral character in certain places, indicating the possible coexistence of mixtures of Fe-rich montmorillonite and saponite. The mechanism of formation of bentonites from basic pyroclastic rocks is not comparable to the low-temperature hydrothermal alteration of basic lavas owing to permeability differences. The pyroclastic precursors of the bentonites have significantly greater permeability compared with the underlying pillow lavas of similar chemistry, favoring leaching of Mg and Ca. Magnesium leaching, coupled with residual enrichment of Fe related to immobility during oxidizing conditions, favored formation of dioctahedral smectite, ferruginous montmorillonite, and beidellite instead of saponite. Indeed the Al_2O_3/Fe_2O_3 ratio is virtually constant in the bentonites derived from basic rocks (Table 3) in accord with the immobility of Al during bentonite formation (Christidis 1998). Moreover the immobility of Fe reflects the oxidizing conditions prevailing on the ocean floor. Similar smectite has been observed during hydrothermal alteration of basalts in the Czech Republic (Cicel et al. 1992). Thus, pervasive alteration of basic volcaniclastic rocks yields Fe-rich montmorillonite or Fe-beidellite. Such rocks are not expected to yield an Al-Mg-rich smectite such as beidellite and Otay-type- and Tatatilla-type montmorillonite owing to the abundance of Fe. The presence of Fe is decisive for the observed compositional heterogeneity of smectites, because it controls the heterogeneity of microenvironmental chemistry. Iron-poor smectites can be more homogeneous regardless of the nature of the parent rock (Christidis 2001, sample FEO-G). In this sense, the Cyprus bentonites are typical examples, in which the parent rock chemistry controls the crystal chemistry of smectites, because the Fe and Al contents of smectite reflect the composition of the parent rock. Pore water composition may modify the smectite chemistry because it dictates the relative abundance of mobile elements such as Mg, Ca, and alkalis, and contributes to microenvironmental heterogeneity.

An interesting result of this study, which corroborates previous reports (cf. Christidis and Dunham 1993, 1997) is the lack of a well-expressed negative relationship either between ^{VI}Al and Mg or between Mg and Fe^{3+} in Al-rich dioctahedral smectites. In fact, Mg is inversely correlated with ^{VI}Al only in Fe-poor smectites, with <0.1 Fe^{3+} atoms phfu (Christidis and Dunham 1997), suggesting that the substitution of ^{VI}Al and Fe^{3+} by Mg may not be favored in natural smectites. Although, this conclusion is at odds with the traditional perception that Mg is an essential element for smectite formation (Harder 1972), the replacement of Al or/and Fe^{3+} by Mg is expected to induce considerable strain in the smectite lattice, owing to the difference in the ionic radii of ^{VI}Al, $^{VI}Fe^{3+}$, and ^{VI}Mg (0.61 Å, 0.63 Å in low spin state, and 0.80 Å, respectively). This fact, in turn, supports the idea that smectite may not be a true thermodynamically stable phase.

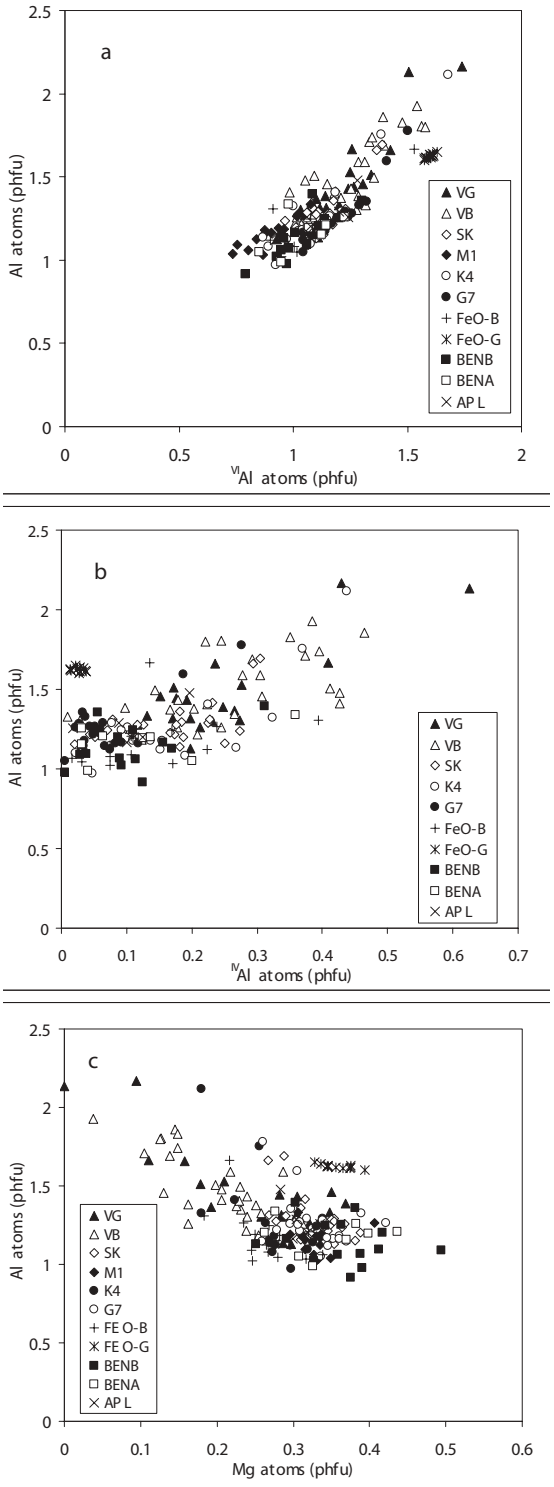

FIGURE 15. Plots showing (**a**) ^{VI}Al vs. Al total, (**b**) ^{IV}Al vs. Al total, and (**c**) Mg vs. Al total in the Cyprus smectite (symbols explained in Fig. 8).

Instead, its formation is controlled by kinetic constraints, being favored by rapid reaction rates over more stable phases such as mica, pyrophyllite, or talc. Nevertheless, the role of Mg is still considered important for smectite formation because it prevents the formation of other phases, such as alkali zeolites, which could inhibit the formation of smectite.

Cyprus smectites display a well-defined positive trend between tetrahedral and total layer charge, and a less well-defined trend between octahedral and total layer charge (Figs. 9a and 9b). This difference indicates that layer charge increases mainly owing to the increase of the beidellitic component. However, most of the analyzed smectites have low Al contents, in contrast to typical beidellite. This apparent inconsistency is explained by the presence of abundant octahedral Fe, which replaces ^{VI}Al (Fig. 8a). The Fe^{3+} for Al substitution does not affect layer charge, whereas Mg-occupancy, which determines the octahedral charge, is considerably smaller than Fe in the smectite studied. Thus tetrahedral sites host a significant fraction of total Al, and ^{IV}Al is an important component of the Cyprus smectite, contributing significantly to layer charge. In this context, the predominance of Fe-rich beidellite in the Moni deposit reflects the greater degree of leaching of Mg relative to Al and Fe, which are immobile. The role of Fe on the distribution of Al in octahedral and tetrahedral sites and the formation either of beidellite or montmorillonite can be visualized further in Figure 15. A well-expressed linear trend holds between total Al and ^{VI}Al (Fig. 15a). The corresponding trend between total Al and ^{IV}Al displays considerable scatter, with Al being constant at lowest concentrations, which corresponds to maximum Fe^{3+} and thus minimum ^{VI}Al abundance, whereas ^{IV}Al increases in the same interval (Fig. 15b). Thus, the ^{IV}Al content (tetrahedral charge) is controlled by the abundance of Fe at a low Al concentration and by the abundance of Al at high-Al concentration. As expected (e.g., Fig. 9c), octahedral Mg behaves opposite to ^{IV}Al (Fig. 15c). Therefore, at lowest total Al contents, although ^{IV}Al increases, montomorillonite forms instead of beidellite owing to the increase of octahedral Mg. Finally, the low Mg contents of samples 1, 13, and 14 are related to the abundance of Si, owing to free SiO_2-polymorphs, either quartz or/and opal CT. Also, the considerable scatter in the trend between total charge and octahedral charge (Fig. 9b) reflects the different degree of leaching of Mg during alteration, because octahedral charge is controlled mainly by the Mg for Al substitution.

The bentonites from the black horizon of the Polycanthos deposit contain significant amounts of MnO, exceeding 3% in some cases. However even at such high-Mn contents, smectite is essentially Mn-free, the main Mn-bearing phase being todorokite. Sherman and Vergo (1988) suggested that although Mn^{3+} can theoretically replace octahedral Fe^{3+} in smectites, owing to their very similar ionic radii, it cannot occupy a significant fraction of octahedral sites for two reasons: first, because Mn^{3+} has limited geochemical stability in most geological environments; and second, because of the large tetragonal distortion of the Mn^{3+} coordination site along the *z*-axis, which induces excess lattice strain. Nevertheless, trioctahedral Mn-rich smectite containing Mn^{2+} has been reported as a primary weathering product of tephroite, which at a later, more evolved stage of weathering converted to Mn-oxyhydroxides (Nahon et al. 1982). Although direct comparison with the aforementioned alteration of tephroite cannot be made owing to the substantially lower Mn-content in the umbers, a similar evolution may have occurred in this study,

i.e., an initial unstable Mn^{2+}-bearing smectite phase, owing to the predominance of oxidizing conditions, may have been converted to ferruginous smectite releasing Mn, which in turn formed todorokite. In any case, the source of Mn was the hydrothermal system, which was circulating in the higher members of the Troodos complex. Therefore, it seems that smectite cannot be a stable main host of Mn even under favorable geochemical conditions characterized by excess Mn.

Influence on the properties of the Cyprus bentonites

Recent work has shown that Cyprus bentonites have rheological and swelling properties that do not meet international specifications, but can be activated successfully with inorganic acids (Christidis and Kosiari 2003). Such properties are related to the mineralogical composition of the bentonites and the crystal-chemical and morphological characteristics of smectite. The bentonites have moderate smectite contents, which render them unsuitable for most of the traditional industrial applications of bentonites because they do not meet international standards. Also, the low dehydroxylation temperature of smectites related to the *trans*-vacant octahedral configuration renders Cyprus bentonites inferior materials for foundry applications owing to the greater need for replacement after use. However, the high-Fe content of the smectites facilitates dissolution during acid activation with inorganic acids such as HCl or H_2SO_4. Therefore, mild acid treatments for short times can increase the specific surface area of the smectites and improve significantly their sorptive properties rendering them efficient decolorizing agents for edible oils.

The significant tetrahedral charge component, coupled with the moderately high layer charge of the smectite (Table 3) predict the observed low swelling capacity of the Cyprus bentonites. All samples except FEO-G, which contains low-charge montmorillonite without tetrahedral charge, develop poor swelling and rheological properties. When tested according to API specifications (API 13B 2003), most bentonites form suspensions with rheological behavior typical of Newtonian fluids, i.e., they do not develop thixotropy and thus are unsuitable for drilling applications (Petavratzi 2000). Moreover, the significant K-component in the exchangeable sites of smectites renders industrial Na-activation (Na-exchange) a difficult task, because K is expected to be associated with those layers having higher layer charge and thus a greater selectivity for K. Also, the predominance of flat smectite flakes and the lack of honeycomb textures indicate in situ face-to-face flocculation of smectite crystallites. Moreover, the existence of halite in most materials studied increases the tendency of bentonite suspensions for flocculation. Indeed, Na-exchange at the laboratory scale does not improve the swelling properties of the Cyprus bentonites significantly (Petavratzi 2000).

ACKNOWLEDGMENTS

Fieldwork was carried out during summer 1999 and 2000. The Hellenic Mining Company (EME) is gratefully acknowledged for their permission to sample their quarries and assistance during fieldwork. G. Katsikis from the Greek Geological Survey (IGME) assisted with the microprobe analyses. The author thanks D.D. Eberl for reviewing the original version of the script and improving the English. The constructive comments of J. Cuadros, W. Huff, and S. Guggenheim improved the text.

REFERENCES CITED

Alt, J.C. (1999) Very low-grade hydrothermal metamorphism of basic igneous rocks. In M. Frey and D. Robinson, Eds., Low grade metamorphism, p. 169–201. Blackwell Science, Oxford.

Alt, J.C. and Honnorez, J. (1984) Alteration of the upper oceanic crust, DSPD site 417: Mineralogy and chemistry. Contribution to Mineralogy and Petrology, 87, 149–169.

Alt, J.C., Teagle, D.A.H., Brewer, T.S., Shanks, W.C., and Halliday, A.N. (1998) Alteration and mineralization of an oceanic forearc and the ophiolite-ocean crust analogy. Journal of Geophysical Research, 103, 12365–12380.

American Petroleum Institute Specifications (API) 13B (2003) Standard Procedure for Testing Drilling Fluids. American Petroleum Institute, Washington, D.C.

Banfield, J.F. and Eggleton, R.A. (1990) Analytical transmission electron microscope studies of plagioclase, muscovite, and K-feldspar weathering. Clays and Clay Minerals, 38, 77–89.

Bennett, H. and Oliver, G.J. (1976) Development of fluxes for the analysis of ceramic materials by X-ray Spectrometry. Analyst, 101, 803–807.

Bishop, J., Madejova, J., Komadel, P., and Fröschl, H. (2002) The influence of structural Fe, Al and Mg on the infrared OH bands in spectra of dioctahedral smectites. Clay Minerals, 37, 607–616.

Boles, J.R. (1972) Composition, optical properties, cell dimensions and thermal stability of some heulandite group zeolites. American Mineralogist, 57, 1463–1493.

Brigatti, M.F. (1983) Relationships between composition and structure in Fe-rich smectites. Clay Minerals, 18, 177–186

Brigatti, M.F. and Poppi, L. (1981) A mathematical model to distinguish the members of the dioctahedral smectite series. Clay Minerals, 16, 81–89.

Christidis, G.E. (1998) Comparative study of the mobility of major and trace elments during alteration of an andesite and a rhyolite to bentonite, in the islands of Milos and Kimolos, Aegean, Greece. Clays and Clay Minerals, 46, 379–399.

——— (2001) Formation and growth of smectites in bentonites: a case study from Kimolos Island, Aegean, Greece. Clays and Clay Minerals, 49, 204–215.

Christidis, G.E. and Dunham, A.C. (1993) Compositional variations in smectites: Part I. Alteration of intermediate volcanic rocks. A case study from Milos Island, Greece. Clay Minerals, 28, 255–273.

——— (1997) Compositional variations in smectites: Part II. Alteration of acidic precursors. A case study from Milos Island, Greece. Clay Minerals, 32, 253–270.

Christidis, G.E. and Eberl, D.D. (2003) Determination of layer charge characteristics of smectites. Clays and Clay Minerals, 51, 644–655.

Christidis, G.E. and Kosiari, S. (2003) Decolorization of vegetable oils: a study of adsorption of β-carotene by an acid activated bentonite from Cyprus. Clays and Clay Minerals, 51, 327–333.

Christidis, G., Scott, P.W., and Marcopoulos, T. (1995) Origin of the bentonite deposits of Eastern Milos, Aegean, Greece: Geological, Mineralogical and Geochemical evidence. Clays and Clay Minerals, 43, 63–77.

Cicel, B., Komadel, P., Bednarikova, E., and Madejova, J. (1992) Mineralogical compostion and distribution of Si, Al, Fe, Mg and Ca in the fine fractions of some Czech and Slovak bentonites. Geologica Carpathica-Series Clays, 1, 3–7.

Cuadros, J., Sainz-Diaz, C.I., Ramirez, R., and Hernandez-Laguna, A. (1999) Analysis of Fe segregation in the octahedral sheet of bentonitic illite-smactite by means of FTIR, ^{27}Al MAS NMR and reverse Monte Carlo simulations. American Journal of Science, 299, 289–308.

Ddani, M., Meunier, A., Zahraoui, M., Beaufort, D., El Wartiti, M., Fontaine, C., Boukili, B., and El Mahi, B. (2005) Clay mineralogy and chemical composition of bentonites from the Gourougou volcanic massif (northeast Morocco). Clays and Clay Minerals, 53, 250–267.

Decarreau, A., Colin, F., Herbillon, A., Manceau, A., Nahon, D., Paquet, H., Trauth-Badeaud, D., and Trescases, J.J. (1987) Domain segregation in Ni-Fe-Mg-smectites. Clays and Clay Minerals, 35, 1–10.

Drits, V.A., Lindgreen, H., Salyn, A.L., Ylagan, R., and McCarty, D.K. (1998) Semi quantitative detrmination of trans-vacant and cis-vacant 2:1 layers in illites and illite-smectites by thermal analysis and X-ray diffraction. American Mineralogist, 83, 1188–1198.

Dunham, A.C. and Wilkinson, F.C.F. (1978) Accuracy, precision and detection limits of energy-dispersive electron microprobe analysis of silicates. X-ray Spectrometry, 7, 50–56.

Gass, I.G. (1980) The Troodos Massif: its role in the unravelling of the ophiolite problem and its significance in the understanding of constructive plate margin processes. In A. Panayiotou, Ed., Ophiolites: International Ophiolite Symposium, Cyprus 1979, p. 23–35. Cyprus, Ministry of Argiculture and Natural Resources, Geological Survey Department.

Gaudin, A., Petit, S., Rose, J., Martin, F., Decarreau, A, Noack, Y., and Borschneck, D. (2004) The accurate crystal chemistry of ferric smectites from the lateritic nickel ore of Murrin Murrin (Western Australia). II. Spectroscopic (IR and

EXAFS) approaches. Clay Minerals, 39, 453–467.
Gillis, K.M. and Robinson, P.T. (1990) Patterns and processes of alteration in the lavas and dykes of the Troodos ophiolite, Cyprus. Journal of Geophysical Research, 95, 21523–21548.
Goulding, K.W.T. and Talibudeen, O. (1980) Heterogeneity of cation-exchange sites for K-Ca exchange in aluminosilicates. Journal of Colloid and Interface Science, 78, 15–24.
Grim, R.E. and Güven, N. (1978) Bentonites. Geology, mineralogy, properties and uses, p. 143–155. Elsevier, Amsterdam.
Grim, R.E. and Kulbicki, G. (1961) Montmorillonite: High temperature reactions and classification. American Mineralogist, 46, 1329–1369.
Güven, N. (1988) Smectite. In S.W. Bailey, Ed., Hydrous Phyllosilicates (Exclusive of Micas), 19, p. 497–559. Reviews in Mineralogy, Mineralogical Society of America, Chantilly, Virginia.
Harder, H. (1972) The role of magnesium in the formation of smectite minerals. Chemical Geology, 10, 31–39.
Hay, R.L. and Sheppard R.A. (2001) Occurrence of zeolites in sedimentary rocks: An overview. In D.L. Bish and D.W. Ming, Eds., Natural zeolites: properties applications and uses, 45, p. 217–232. Reviews in Mineralogy and Geochemistry, Mineralogical Society of America, Chantilly, Virginia.
Iwazaki, T. and Watanabe, T. (1988) Distribution of Ca and Na ions in dioctahedral smectites and interstratified dioctahedral mica/smectites. Clays and Clay Minerals, 36, 73–82.
Jeans, C.V., Merriman, R.J., and Mitchell, J.G. (1977) Origin of Middle Jurassic and Lower Cretaceous Fuller's Earths in England. Clay Minerals, 12, 11–44.
Jones, J.B. and Segnit, E.R. (1971) The nature of opal. I Nomenclature and constituent phases. Journal of the Geological Society of Australia, 18, 57–68.
Khoury, H.N. and Eberl, D.D. (1982) Bubble-wall shards altered to montmorillonite. Clays and Clay Minerals, 27, 291–292.
Köster, H.M. (1982) The crystal structure of 2:1 Layer silicates. Proceedings of International Clay Conference Pavia, Italy, 41–71. Elsevier, Amsterdam.
Köster, H.M., Ehrlicher, U., Gilg, H.A., Jordan, R., Murad, E., and Onnich, K. (1999) Mineralogical and chemical characteristics of five nontronites and Fe-rich smectites. Clay Minerals, 34, 579–599.
Lagaly, G. and Weiss, A. (1975) The layer charge of smectitic layer silicates. In S.W. Bailey, Ed., Proceedings of International Clay Conference, Mexico, p. 157–172. Applied Publishing Ltd., Wilmette, Illinois.
Lagaly, G., Fernandez-Gonzalez, M., and Weiss, A. (1976) Problems in layer-charge determination of montmorillonites. Clay Minerals, 11, 173–187.
Lim, C.H. and Jackson, M.L. (1986) Expandable phyllosilicate reactions with lithium on heating. Clays and Clay Minerals, 34, 346–352.
Lippmann, F. (1982) The thermodynamic status of clay minerals. In H. van Olphen and F. Veniale, Eds., Proceedings of the International Clay Conference Pavia, Italy, p. 475–485. Elsevier, Amsterdam.
Madejova, J. and Komadel, P. (2001) Baseline studies of the Clay Mineral Society source clays: Infrared methods. Clays and Clay Minerals, 49, 410–432.
Matsuda, H., O'Neil, J.R., Jiang, W.-T., and Peacor, D.R. (1996) Relation between interlayer composition of authigenic smectite, mineral assemblages, I/S reaction rate and fluid composition of silicic ash of the Nankai Trough. Clays and Clay Minerals, 44, 443–459.
May, H.M., Kinniburgh, D.G., Helmke, P.A., and Jackson, M.L. (1986) Aqueous dissolution, solubilities and thermodynamic stabilities of common aluminosilicate clay minerals; kaolinite and smectite. Geochemica et Cosmochimica Acta, 50, 1667–1677.
Meunier, A. and Velde, B. (1989) Solid solutions in I/S mixed layer minerals and illite. American Mineralogist, 74, 1106–1112.
Moores, E.M., Robinson, P.T., Malpas, J., and Xenophontos, C. (1984) A model for the origin of the Troodos Massif, Cyrus and other mid-east ophiolites. Geology, 12, 500–503.
Mukasa, S.B. and Ludden, J.N. (1987) Uranium-lead isotopic ages of plagiogranites from the Troodos ophiolite, Cyprus and their tectonic significance. Geology, 15, 825–828.
Nadeau, P.H, Farmer, V.C., McHardy, W.J., and Bain, D.C. (1985) Compositional variations of the Unterrupsroth beidellite. American Mineralogist, 70, 1004–1010.
Nahon, D., Colin, F., and Tardy, Y. (1982) Formation and distribution of Mg, Fe, Mn- smectites in the first stages of the lateritic weathering of forsterite and tephroite. Clay Minerals, 17, 339–348.
Newman, A.C.D. and Brown, G. (1987) The chemical constitution of clays. In A.C.D Newman, Ed., Chemistry of Clays and Clay Minerals, p. 1–128. Mineralogical Society, London.
Odin, G.S., Despairies, A., Fullagar, P.D., Bellon, H., Decarreau, A., Fröhlich, F., and Zelveder, M. (1988) Nature and geological significance of celadonite. In G.S. Odin, Ed., Green Marine Clays, vol. 45, p. 337–398. Developments in Sedimentology, Elsevier Science, Amsterdam.
Paquet, H., Duplay, J., and Nahon, D. (1982) Variations in the composition of phyllosilicates monoparticles in a weathering profile of ultrabasic rocks. In H. van Olphen and F. Veniale, Eds., Proceedings of the International Clay Conference Pavia, Italy, p. 595–603. Elsevier, Amsterdam.
Pearce, J.A. (1980) Geochemical evidence for the genesis and eruptive setting of lavas from Tethyan ophiolites. In A. Panagiotou, Ed., Ophiolites. Proceedings of the International Ophiolite Symposium, Cyprus 1979, p. 261–272. Ministry of Agriculture and Natural Resources, Geological Survey Department. Cyprus.
Petavratzi, E. (2000) Study of the bentonite deposit of Polycanthos, Cyprus. Unpublished Diploma Thesis, Technical University of Crete, Greece, p. 112 (in Greek).
Reynolds, R.C., Jr. and Reynolds, R.C., III (1996) Newmod for Windows. The calculation of one-dimensional X-ray diffraction patterns of mixed-layer clay minerals. Hanover, New Hampshire.
Robinson, P.T., Melson, W., and Schmincke, H.-U. (1983) Volcanic glass compositions of the Troodos ophiolite. Geology, 11, 400–404.
Russell, J.D. and Clarke, D.R. (1978) The effect of Fe-for-Si substitution on the *b*-dimension of nontronite. Clay Minerals, 13, 133–137.
Schultz, L.G. (1969) Lithium and potassium adsorption, dehydroxylation temperature and structural water content of aluminous smectites. Clays and Clay Minerals, 17, 115–149.
Sherman, D.M. and Vergo, N. (1988) Optical spectrum, site occupancy, and oxidation state of Mn in montmorillonite. American Mineralogist, 73, 140–144.
Shiraki, R. and Iiyama, T. (1990) Na-K ion exchange reaction between rhyolitic glass and (Na,K)Cl aqueous solution under hydrothermal conditions. Geochimica et Cosmochimica Acta, 54, 2923–2931.
Spooner, E.T.C., Chapman, H.J., and Smewing, J.D. (1977) Strontium isotopic contamination and oxidation during ocean floor hydrothermal metamorphism of the opiolitic rocks of the Troodos Massif, Cyprus. Geochimica et Cosmochimica Acta, 41, 873–890.
Staudigel, H. and Gillis, K.M. (1991) The timing of hydrothermal alteration in the Troodos ophiolite. In E.M. Moores and A. Panayiotou, Eds., Troodos '87: Ophiolites and Oceanic lithosphere, p. 665–672. Geological Survey Department, Nicosia, Cyprus.
Talibudeen, O. and Goulding, K.W.T. (1983) Charge heterogeneity in smectites. Clays and Clay Minerals, 31, 37–42.
Tettenhorst, R. and Johns, W.D. (1966) Interstratification in montmorillonite. Clays and Clay Minerals, 25, 85–93.
Thy, P. (1987) Petrogenetic implications of mineral crystallization trends of Troodos cumulates, Cyprus. Geological Magazine, 124, 1–11.
Velde, B. (1984) Electron microprobe analysis of clay minerals. Clay Minerals, 19, 243–247.
Weaver, C.E. and Pollard, L.D. (1973) The chemistry of clay minerals, p. 55–77. Elsevier, Amsterdam.
Winchester, J.A. and Floyd, P.A. (1977) Geological discrimination of different magma series and their differentiation products using immobile elements. Chemical Geology, 20, 325–343.
Zhou, Z. and Fyfe, W.S. (1989) Palagonization of basaltic glass of DSPD Site 335, Leg 37: Textures, chemical composition and mechanism of formation. American Mineralogist, 74, 1045–1053.

MANUSCRIPT RECEIVED JUNE 8, 2005
MANUSCRIPT ACCEPTED SEPTEMBER 13, 2005
MANUSCRIPT HANDLED BY STEPHEN GUGGENHEIM